The Meteoritical Society

Meteoritics & Planetary Science 48, Nr 3, 493–513 (2013)
doi: 10.1111/maps.12074

The Ksar Ghilane 002 shergottite—The 100th registered Martian meteorite fragment

Jordi LLORCA[1,2*], Julia ROSZJAR[3], Julia A. CARTWRIGHT[4,#], Addi BISCHOFF[3], Ulrich OTT[4,5], Andreas PACK[6], Silke MERCHEL[7], Georg RUGEL[7], Leticia FIMIANI[8], Peter LUDWIG[8], José V. CASADO[9], and David ALLEPUZ[9]

[1]Institut de Tècniques Energètiques, Universitat Politècnica de Catalunya, Diagonal 647, ed. ETSEIB, Barcelona 08028, Spain
[2]Centre for Research in Nanoengineering, Universitat Politècnica de Catalunya, Pasqual i Vila 15, Barcelona 08028, Spain
[3]Institut für Planetologie, Westfälische Wilhelms-Universität Münster, Wilhelm-Klemm-Str. 10, Münster 48149, Germany
[4]Max Planck Institut für Chemie, Hahn-Meitner-Weg 1, Mainz 55128, Germany
[5]University of West Hungary, Szombathely 9700, Hungary
[6]Universität Göttingen, Geowissenschaftliches Zentrum, Goldschmidtstrasse 1, Göttingen 37077, Germany
[7]Helmholtz-Zentrum Dresden-Rossendorf, Dresden 01314, Germany
[8]Technische Universität München, Garching 85748, Germany
[9]Sant Julià de Vilatorta Observatory, Barcelona, Spain
[#]Present address: Division of Geological and Planetary Sciences, California Institute of Technology, MC 100-23, 1200 E. California Blvd., Pasadena, California 91125, USA
[*]Corresponding author. E-mail: jordi.llorca@upc.edu

(Received 28 December 2011; revision accepted 01 January 2013)

Abstract–We report on the discovery of a new shergottite from Tunisia, Ksar Ghilane (KG) 002. This single stone, weighing 538 g, is a coarse-grained basaltic shergottite, mainly composed of maskelynitized plagioclase (approximately 52 vol%) and pyroxene (approximately 37 vol%). It also contains Fe-rich olivine (approximately 4.5 vol%), large Ca-phosphates, including both merrillites and Cl-apatites (approximately 3.4 vol%), minor amounts of silica or SiO_2-normative K-rich glass, pyrrhotite, Ti-magnetite, ilmenite, and accessory baddeleyite. The largest crystals of pyroxene and plagioclase reach sizes of approximately 4 to 5 mm. Pyroxenes ($Fs_{26–96}En_{5–50}Wo_{2–41}$). They typically range from cores of about $Fs_{29}En_{41}Wo_{30}$ to rims of about $Fs_{68}En_{14}Wo_{17}$. Maskelynite is $Ab_{41–49}An_{39–58}Or_{1–7}$ in composition, but some can be as anorthitic as An_{93}. Olivine ($Fa_{91–96}$) occurs mainly within symplectitic intergrowths, in paragenesis with ilmenite, or at neighboring areas of symplectites. KG 002 is heavily shocked (S5) as indicated by mosaic extinction of pyroxenes, maskelynitized plagioclase, the occurrence of localized shock melt glass pockets, and low radiogenic He concentration. Oxygen isotopes confirm that it is a normal member of the SNC suite. KG 002 is slightly depleted in LREE and shows a positive Eu anomaly, providing evidence for complex magma genesis and mantle processes on Mars. Noble gases with a composition thought to be characteristic for Martian interior is a dominant component. Measurements of ^{10}Be, ^{26}Al, and ^{53}Mn and comparison with Monte Carlo calculations of production rates indicate that KG 002 has been exposed to cosmic rays most likely as a single meteoroid body of 35–65 cm radius. KG 002 strongly resembles Los Angeles and NWA 2800 basaltic shergottites in element composition, petrography, and mineral chemistry, suggesting a possible launch-pairing. The similar CRE ages of KG 002 and Los Angeles may suggest an ejection event at approximately 3.0 Ma.

INTRODUCTION

Shergottites, nakhlites, and chassignites (SNC), and Allan Hills (ALH) 84001 meteorites are igneous rocks believed to have originated from Mars. In the past and at present, Martian rocks have been studied extensively to provide possible petrologic constraints on the geological history of Mars (e.g., McSween 1994, 2002). Among the major group of Martian rocks, the shergottites, three subtypes can be distinguished: (1) basaltic shergottites, e.g., Shergotty, Zagami, Queen Alexandra Range (QUE) 94201, Los Angeles, Northwest Africa (NWA) 2800, which are pyroxene-plagioclase-dominated basalts; (2) lherzolitic shergottites, e.g., Allan Hills (ALH) A77005, Lewis Cliff (LEW) 88516, Yamato (Y)-793605 that are olivine-pyroxene cumulates derived from a basaltic magma (McSween and Treiman 1998); and (3) olivine-phyric shergottites, e.g., Dar al Gani (DaG) 476, Dhofar 019, Y-980459, Sayh al Uhaymir (SAU) 005, Elephant Moraine (EET) Lithology A A79001 (Goodrich 2002). The origin of the latter is controversially discussed. They might be products of mixing between basaltic shergottite-like magma sources and lherzolitic material, or represent magmas that could have been parental to both (1) and (2), or may be the product of a completely different magma source and/or formation process. This article addresses petrologic, mineral and bulk chemical, cosmogenic radionuclide, noble gas, and oxygen isotope data of a new basaltic shergottite, Ksar Ghilane 002 (KG 002). This meteorite is the 100th registered fragment available from Mars, not taking paired stones into account, and the first to be recovered from Tunisia. The Sahara has become one of the most productive areas for Martian meteorite recovery, providing nearly half of the collection (101 total; The Meteoritical Bulletin Database, December 2011). In the last 10 years, 50 new fragments have been recovered, 35 of them in the Sahara. Such new discoveries thus present an opportunity to improve our knowledge of Martian meteorites.

Ksar Ghilane 002 was collected by José Vicente Casado and David Allepuz on January 13, 2010, in the Ksar Ghilane dense collection area (KG) at latitude 32°48.375′ N and longitude 009°49.970′ E (Fig. 1a). The find site is on the Saharan platform, over Senonian limestone. The meteorite is a single stone weighing 538 g, with dimensions of approximately 10 × 4.5 × 3.5 cm (Fig. 1b). The surface of KG 002 has been subject to hot desert weathering (i.e., sand abrasion), resulting in the removal of the majority of the fusion crust. In hand sample, KG 002 is dominated by light green pyroxene crystals, abundant maskelynite, and rare opaque oxides (sawn surface shown in Fig. 1c). During the fourth meteorite recovery campaign in Tunisia (2011), although the KG 002 recovery area was carefully examined, no further shergottite specimens were found. Most of our results are discussed with and compared with previous data for two other Martian meteorites—Los Angeles and NWA 2800—as both of them have strong similarities to KG 002. The possibility of a launch-pairing among these basaltic shergottites is also discussed.

ANALYTICAL METHODS

Textural and mineralogical investigations of KG 002 were performed by optical and electron microscopy on four different thin sections. Detailed petrographic investigations were carried out using (1) a JEOL 6610-LV scanning electron microscope (SEM) equipped with energy dispersive spectrometers (EDS; INCA; Oxford Instruments) at the Interdisciplinary Center for Electron Microscopy and Microanalysis (ICEM) at the Westfälische Wilhelms-Universität Münster using an acceleration voltage of 20 kV and a beam current of 15 nA; and (2) a Zeiss Neon 40 field emission SEM equipped with EDS at the Centre for Research in Nanoengineering (CRnE) at the Universitat Politècnica de Catalunya. Quantitative analyses of mineral compositions were obtained using a JEOL JXA 8900 Superprobe electron probe micro-analyzer (EPMA) operated at an acceleration voltage of 15 kV and beam current of 15 nA for major and minor elements (Westfälische Wilhelms-Universität Münster). Shock melt glasses and phosphates have been analyzed with a defocused beam of 50 and 10 μm, respectively. Natural and synthetic standards were used for calibration purposes. These include jadeite (Na), sanidine (K), hypersthene (Si), disthene (Al), olivine (San Carlos, Mg), diopside (Ca), fayalite (Fe), rutile (Ti), rhodonite (Mn), and Cr_2O_3 (Cr). Matrix corrections were made according to the $\Phi\rho(z)$ procedure of Armstrong (1991). The modal mineral abundance of KG 002 was obtained by quantitative electron microprobe grid analysis. A total of 735 points were analyzed and the calculated average of these quantitative data was used to evaluate the major element bulk composition.

A 2.065 g fragment from the interior of the meteorite (at least 1 cm away from the surface in all directions) was finely ground using an agate mortar and pestle. Four aliquots of 79.94, 77.79, 61.94, and 58.01 mg of the powdered specimen were used for bulk chemical analyses. Two independent methods were used for sample preparation: acid digestion treatment in a sealed Teflon reactor and alkaline fusion in a zirconium crucible. Analyses were performed by means of

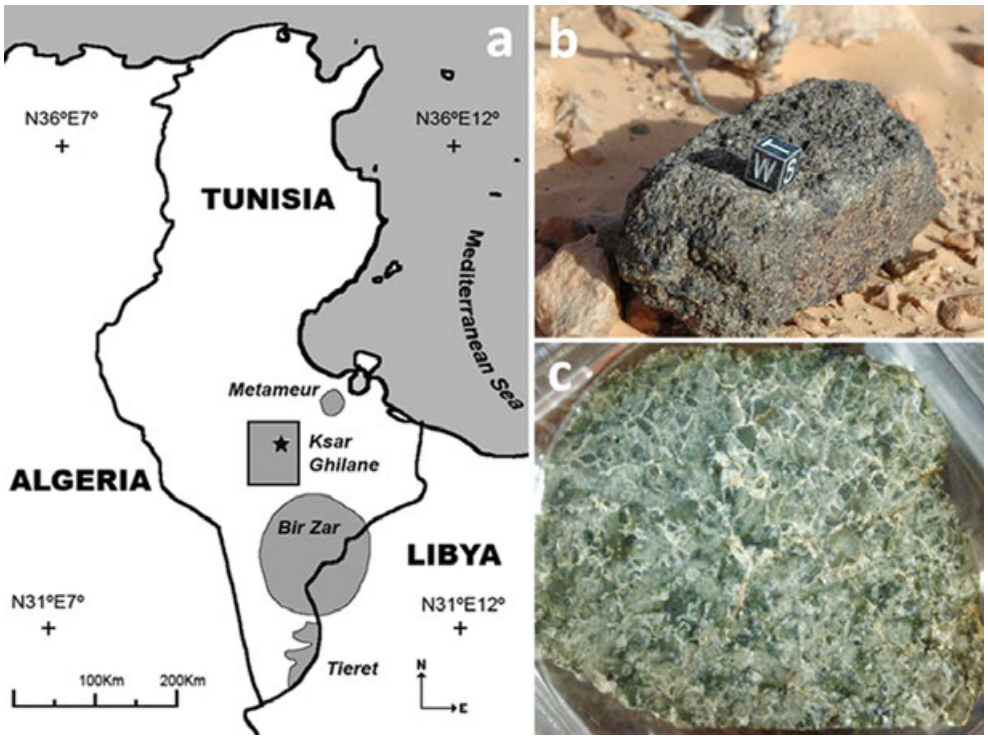

Fig. 1. a) Map of Tunisia showing the location the Ksar Ghilane dense collection area and the discovery location of KG 002. b) The KG 002 shergottite as it was encountered. c) Sawn surface of KG 002 (width of view is approximately 3 cm).

inductively coupled plasma-mass spectrometry (ICP-MS) using a Perkin Elmer Elan 6000 instrument and inductively coupled plasma-optical emission spectroscopy (ICP-OES) using a Perkin Elmer Optima 3200 RL instrument (Barcelona). Our procedures are the same as those described by Llorca et al. (2007, 2009). The accuracy on major and trace element concentrations is better than 5% in all cases.

The oxygen isotope composition was analyzed by means of laser fluorination in combination with gas chromatography continuous flow isotope ratio monitoring mass spectrometry (GC-CF-irmMS). Approximately 1 mg of bulk powder was loaded, along with terrestrial MORB glass ($\delta^{18}O = +5.6‰$) and NBS-28 quartz ($\delta^{18}O = +9.6‰$) standards. The material was fluorinated in a stainless steel sample chamber (Sharp 1990) using approximately 20 mbar purified F_2 gas (Asprey 1976). A SYNRAD 50 W CO_2 laser was used for the heat source. The samples reacted with the F_2 to produce fluorides and O_2. Excess F_2 was removed by reacting the gas mixture with hot (approximately 150 °C) NaCl to form NaF and Cl_2. The Cl_2 was removed in a cold trap (−196 °C) and the sample O_2 was collected in a 13X molecular sieve (−196 °C), which was then released at approximately 150 °C into a He carrier gas stream and transported to a molecular sieve cryofocusing trap (−196 °C). From there, the sample gas was released by submersion in a water bath (92 °C) and transported with He through a THERMO GASBENCH II gas chromatograph (5 Å molecular sieve) and an open split into the source of a THERMO MAT253 multicollector gas mass spectrometer. The gas chromatograph separated interfering NF (from NF_3) (Pack et al. 2007) from O_2. The reference gas was injected using the GASBENCH. The $\delta^{17}O$ and $\delta^{18}O$ values were determined by simultaneously analyzing $m/z = 32$, 33, and 34. The $\Delta^{17}O$ was calculated according to:

$$\Delta^{17}O = 1000\left(\left(\frac{\ln\delta^{17}O}{1000}+1\right) - 0.5251\left(\frac{\ln\delta^{18}O}{1000}+1\right)\right)$$

The $\Delta^{17}O$ of NBS28 quartz and MORB glass was assumed to be zero. The external accuracy of GC-CF-irmMS was ±0.2‰ (1σ) for $\delta^{18}O$ and the external accuracy of $\Delta^{17}O$ (Young et al. 2002) was ±0.05‰ (1σ).

A 67.53 mg bulk fragment of KG 002 was analyzed for all noble gases helium (He), neon (Ne), argon (Ar), krypton (Kr), and xenon (Xe) using an MAP 215-50 noble gas electron source mass spectrometer based at the Max-Planck-Institut für Chemie (MPIC), Mainz. Noble

gases were released from the sample using a furnace step-heating technique in steps of 600, 1000, and 1800 °C. Whilst a final 1900 °C step was performed to ensure that all gases had been released from the sample, this information is omitted from the final results, as in all cases, it was equivalent to a blank. Upper limits on blanks were: ^{4}He 4.4×10^{-10} ccSTP, ^{22}Ne 2.4×10^{-12} ccSTP, ^{36}Ar 9×10^{-12} ccSTP, ^{84}Kr 0.3×10^{-12} ccSTP, ^{132}Xe 0.2×10^{-12} ccSTP. Sensitivity and mass discrimination of the instrument were monitored with analysis of a calibration gas of known composition (standard atmospheric, except for ^{3}He/^{4}He approximately 1), and the data were corrected for interference masses.

Long-lived cosmogenic radionuclides were separated from a 177.44 mg bulk fragment following a procedure described by Merchel and Herpers (1999). Basic steps were: crushing; addition of stable isotope carrier (^{9}Be, ^{35}Cl (^{35}Cl = 99%), ^{55}Mn); acid digestion in a Teflon pressure bomb; anion and cation exchange; precipitation of AgCl, $Be(OH)_2$, $Al(OH)_3$, $MnO(OH)_2$, and $Fe(OH)_3$; drying and partial oxidation (BeO, Al_2O_3, MnO_2, Fe_2O_3); and mixing with metal powder (BeO with Nb; Al_2O_3, MnO_2 and Fe_2O_3 with Ag). Accelerator mass spectrometry (AMS) measurements of ^{10}Be and ^{26}Al were performed at the new 6 MV AMS-facility DREAMS in Dresden (Germany) (Akhmadaliev et al. 2013), whereas ^{53}Mn was detected at the Maier-Leibnitz-Laboratory (MLL) in Garching (Germany) (Poutivtsev et al. 2010). Additionally, ^{60}Fe was determined at MLL (Knie et al. 2000). Calibration materials are SMD-Be-12 with $^{10}Be/^{9}Be = (1.704 \pm 0.030) \times 10^{-12}$, SMD-Al-11 with $^{26}Al/^{27}Al = (9.66 \pm 0.14) \times 10^{-12}$, Grant GLS with $^{53}Mn/^{55}Mn = (2.83 \pm 0.14) \times 10^{-10}$, and PSI-12 with $^{60}Fe/Fe = (1.25 \pm 0.13) \times 10^{-12}$ diluted from a primary standard (Rugel et al. 2009). Both DREAMS calibration materials are traceable to primary standard-type materials, i.e., via cross-calibration to NIST SRM 4325 (Nishiizumi et al. 2007) and the ^{26}Al round-robin material of Merchel and Bremser (2004). Grant GLS is an in-house calibration material traceable to a primary-type standard resulting from a nuclear reaction (Schaefer et al. 2006). However, the original published value of $(2.96 \pm 0.06) \times 10^{-10}$ (Schaefer et al. 2006) has been slightly changed due to advanced cross-calibration measurements. Used ^{26}Al and ^{53}Mn standards are generally independent from a certain half-life. Half-lives used for the conversion of isotope ratios into radionuclide activities are (1.387 ± 0.012) Ma for ^{10}Be (Korschinek et al. 2010), (0.705 ± 0.024) Ma for ^{26}Al (Norris et al. 1983), and (3.7 ± 0.4) Ma for ^{53}Mn (Honda and Imamura 1971). Measured concentrations have been compared with depth- and radius-depending production rates from theoretical Monte Carlo calculations (Leya and Masarik 2009) based on the mean bulk chemical composition of KG 002.

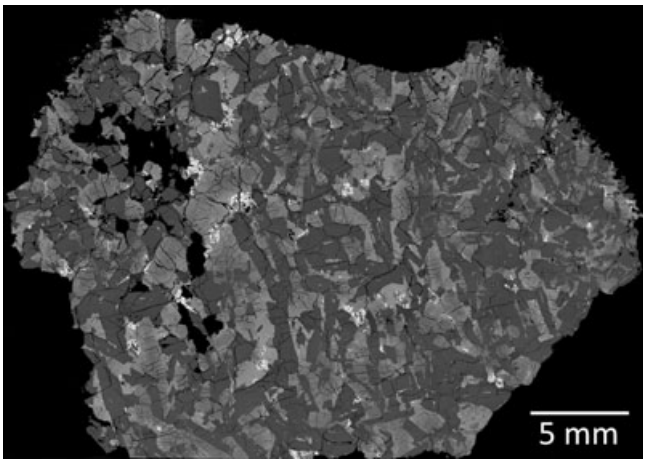

Fig. 2. Backscattered electron image of a whole polished section of KG 002 showing dominant maskelynite (dark gray), pyroxene (light gray), and oxides (white).

RESULTS AND DISCUSSION

Petrography and Mineral Chemistry

Our analyses indicate that KG 002 is a coarse-grained basaltic shergottite with an ophitic to subophitic texture and preferred orientation of large, elongated grains (Figs. 2 and 3). It is mainly composed of maskelynitized plagioclase (approximately 52 vol%) and pyroxene (approximately 37 vol%), with Ca-phosphates, including both merrillite and Cl-apatite, minor amounts of silica or SiO_2-normative K-rich glass, Fe-rich olivine, pyrrhotite, Ti-magnetite, ilmenite, and trace amounts of baddeleyite (Table 1). The largest crystals of pyroxene and plagioclase in KG 002 reach sizes of approximately 4 and 5 mm, exceeding those of most other basaltic shergottites including Los Angeles (e.g., Mikouchi 2000), except for NWA 2800 (Bunch et al. 2008). The latter strongly resembles KG 002 in texture, grain sizes, and mineral constituents. The bulk rock chemical composition for major elements (calculated based on EPMA data), and representative analyses of silicates and oxides in KG 002 are given in Tables 2 and 3.

The large plagioclases (maskelynite) are $An_{37–58}Or_{1–7}Ab_{41–59}$ in composition (Table 3), whereas the smaller ones, which are interstitial to pyroxenes or in close association with melt pockets, can be as anorthitic as An_{93}. The maskelynite composition is significantly distinct from that of highly evolved NWA 2800 ($An_{55.5–72.3}Or_{0.6–3.8}$; Bunch et al. 2008), but similar to maskelynite in Los Angeles ($An_{38–56}Or_{1–7}Ab_{43–56}$; Rubin et al. 2000)

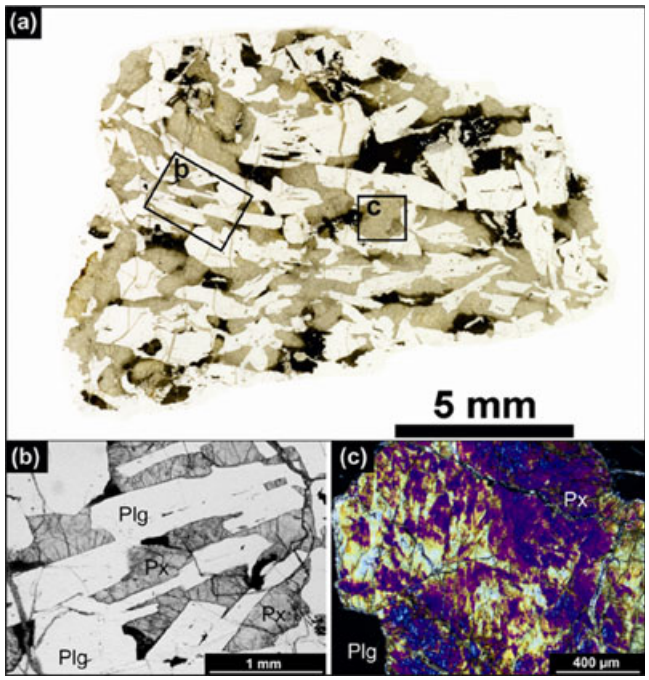

Fig. 3. a) Photomicrograph of a thin section illustrating the coarse-grained basaltic texture of KG 002 with dominating portion of maskelynite (clear), large pyroxene crystals (tan) with preferred orientation, and mm-sized glass and symplectite patches (black). b) Representative close-up photomicrograph of the coarse-grained basaltic texture, composed of mm-sized plagioclase (Plg) and pyroxene (Px) grains. c) Close-up image of a pyroxene crystal, obtained with crossed-polarized light, illustrating mosaic extinction as indication for shock.

and Shergotty ($An_{41–56}Or_{1–3}Ab_{41–56}$; Smith and Hervig 1979). In addition to maskelynite and smaller plagioclase crystals, amorphous K-feldspars were found to occur within SiO_2-normative glass patches together with accessory pyroxene and pyrrhotite (Fig. 4b). Their composition can be calculated as $An_{24–43}Or_{5–34}Ab_{38–57}$ (Table 3) and thus differs from surrounding plagioclase (or maskelynite). It is likely that both the K-feldspar and SiO_2-phases have been converted into an amorphous state during shock metamorphism.

The pyroxenes in KG 002 are strongly zoned and typically crosscut by numerous cracks (Fig. 3). Their compositions range from $Fs_{26–96}En_{3–50}Wo_{2–41}$, with Mg-rich cores of about $Fs_{29}En_{41}Wo_{30}$ to Fe-rich rims of about $Fs_{68}En_{14}Wo_{18}$ (Table 3, Figs. 5 and 6). This zoning is clearly indicated in Figs. 5d and 5f. The range of pyroxene composition, given in Fig. 6, is similar to that of Los Angeles pyroxenes (Mikouchi 2001; Xirouchakis et al. 2002). Approximately 10–15 vol% of the KG 002 sample consists of 50 µm to 2 mm wide patches of a fine-grained vermicular to microgranulitic intergrowth of fayalite, Ca-pyroxene, and silica, in approximately 2:2:1 proportion (Figs. 4c and 5c), a texture previously described as symplectite (e.g.,

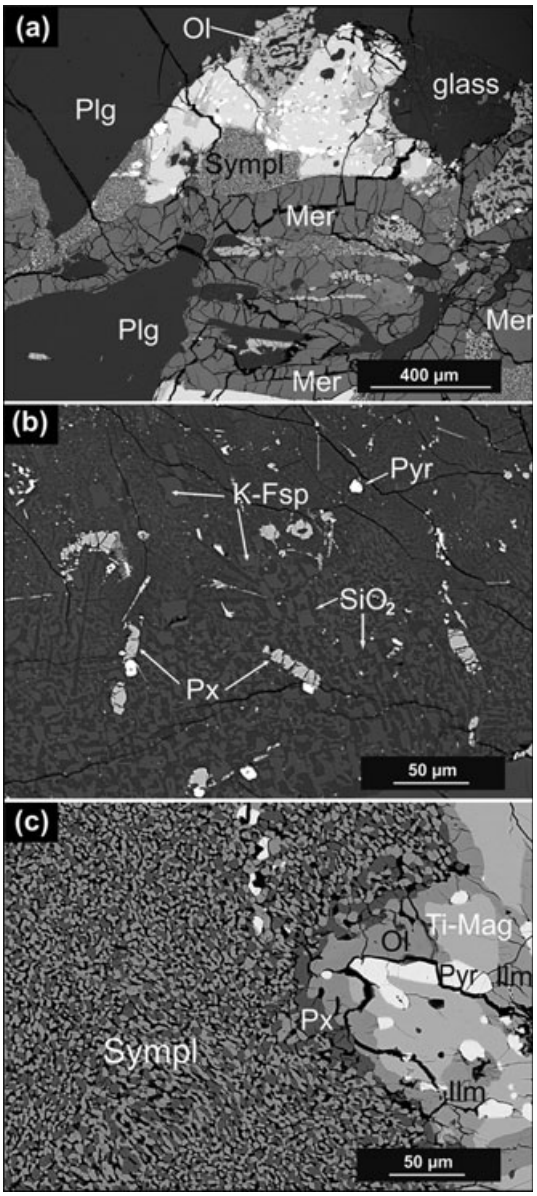

Fig. 4. Detailed BSE images of: a) a large merrillite grain (Mer), intergrown with plagioclase (Plg), olivine (Ol), oxides (ilmenite (white), and pyrrhotite (light gray)) with interstitial symplectite (Sympl), and a SiO_2-normative K-feldspar-bearing glass patch. The latter is shown in (b) in a close-up view. K-feldspars (K-Fsp) occur as blocky crystals in a SiO_2-normative glass with traces of pyrrhotite (Pyr) and pyroxene (Px). c) Fine-grained intergrowth composed of Fe-rich olivine (light gray), Ca-pyroxene (dark gray), and a silica phase (black), termed symplectite (Sympl), with bordering pyroxene (Px), olivine (Ol), ilmenite (Ilm), Ti-magnetite (Ti-Mag), and pyrrhotite (Pyr).

Aramovich et al. 2002). As already proposed by Lindsley et al. (1972), such symplectites may have formed due to the breakdown of pyroxferroite at low pressure and during slow cooling, coupled with a ferroan bulk composition of the host rock. Overall, the

Table 1. Modal abundance of major phases (vol%).

	KG 002[a]		Los Angeles			
		(1)	(1)	(2)	(3)	NWA 2800 (4)[c]
Plagioclase (maskelynite)	51.7	43.6	44.8	45.0	53.9 ± 3.2	47
Pyroxene	36.7	37.7	43.7	41.6	40.9 ± 2.8	39
Silica (or SiO_2-normative, often K-rich areas)	2.6	4.9	2.4	2.7	1.7 ± 0.2	2
Fa-rich olivine	4.5	4.2	1.9	1.9	–	
K-feldspar (or glass)	–	2.4	1.6	3.7	–	
Ca-phosphates	3.4	2.7	2.4	2.3	1.0 ± 0.1	
Pyrrhotite	0.3	0.7	0.6	–	–	
Oxides	0.8	3.7	2.4	1.7[b]	1.0 ± 0.1	2

[a]Based on EPMA analyses: 735 points; (1) Rubin et al. (2000), two stone fragments analyzed; (2) Mikouchi (2001); (3) Xirouchakis et al. (2002; including 1.5 vol% fusion crust).
[b]Ulvöspinel and ilmenite and 1.1 vol% other phases. (4) Connolly et al. (2008).
[c]Including 10 vol% decomposed patches, and 2 vol% late stage residuum, with the latter probably equivalent to SiO_2-normative, K-rich areas.

Table 2. Chemical composition. Results in wt%.

	KG 002		Los Angeles					Dhofar 378
	(1)	(2)	(3)	(3)	(4)	(5)	(5)	(6)
SiO_2	49.1	50.99	49.1	48.6	–	48.3	47.4	48.08
TiO_2	0.4	0.93	1.30	1.43	1.12	0.92	1.29	1.18
Al_2O_3	14.1	12.25	11.2	10.4	10.86	9.7	9.46	9.5
Cr_2O_3	–	0.02	0.012	0.015	0.015	–	–	–
FeO	14.3	16.96	21.2	21.4	21.07	21.5	24.2	21.11
MnO	0.38	0.43	0.45	0.47	0.46	0.52	0.57	0.55
CaO	12.8	10.30	9.95	9.89	9.92	10.32	9.64	9.76
MgO	4.2	4.47	3.53	3.74	3.91	5.11	3.53	5.35
Na_2O	2.78	2.14	2.22	2.13	2.24	1.86	2.02	2.31
K_2O	0.24	0.23	0.24	0.31	0.36	0.15	0.19	0.15
P_2O_5	1.5	0.70	0.66	1.49	–	1.08	1.26	0.9
S	0.1	0.19	–	–	–	–	–	–

(1) This study, calculated from EPMA data normalized to 100%, P_2O_5- and S-concentrations calculated from modal abundance of phosphates and pyrrhotite; (2) This study, data obtained by ICP-MS and ICP-OES (Si); (3) Rubin et al. (2000; INAA); (4) Jambon et al. (2002; ICP/AES); (5) Warren et al. (2000; electron microprobe); (6) Ikeda et al. (2006; electron microprobe).

modal abundance and composition of these symplectite areas are similar to those described for Los Angeles and NWA 2800 (Rubin et al. 2000; Aramovich et al. 2002; Bunch et al. 2008). However, the apparent size of these patches is significantly larger (up to 2 mm) compared with other shergottites.

Olivine, which constitutes about 4.5 vol% of the whole rock (Table 1), occurs mainly within symplectitic intergrowths, in paragenesis with ilmenite and Ca-phosphates, or at neighboring areas of symplectites (Figs. 4a, 4c, 5b, and 5c). Olivine crystals are $Fa_{91–96}$ in composition and thus comparable to those described in the Los Angeles shergottite ($Fa_{93–95}$; Xirouchakis et al. 2002).

Ca-phosphates, including both merrillite and Cl-apatite, are abundant in KG 002 and represent about 3.4 vol% of the whole rock (Table 1). However, the dominating phase is merrillite, with crystal sizes up to 800 μm in apparent diameter (Figs. 4a and 5c). Their average composition is given in Table 3. Fe-Ti oxides, including Ti-magnetite and ilmenite, typically occur interstitial to pyroxenes and plagioclase or are associated with phosphates and symplectite areas (Figs. 4a, 4c, and 5c). Coexisting Fe-Ti oxide compositions indicate oxygen fugacity equilibrium of the rock near the quartz-fayalite-magnetite buffer (McSween 1994). Baddeleyite is present as an accessory phase within KG 002. The grains are usually <5 μm in diameter with the largest grain being 15 × 10 μm in apparent size, and typically occur at the edges of symplectite areas, as enclosed crystals in Ti-magnetite and in close association with merrillite.

Table 3. Chemical composition of silicates and oxides obtained with EPMA. Results in wt%.

	Pyroxenes $n = 82$	Maskelynite $n = 36$	Amorph. Fsp in SiO_2-normative glass[a] $n = 17$	Olivine $n = 16$	Merrillite $n = 17$	Cl-apatite[d] $n = 24$	Silica $n = 12$	Ilmenite $n = 8$	Ti-magnetite $n = 14$		Pyrrhotite $n = 20$
Na_2O	0.20	5.2	4.7	0.07	1.25	0.10	0.16	<0.02	0.07	Na	<0.01
MgO	8.4	0.08	<0.01	2.32	1.00	<0.04	<0.01	0.18	0.12	Mg	<0.01
Al_2O_3	1.25	26.1	23.3	0.19	<0.04	0.13	1.16	<0.04	1.81	Si	<0.01
SiO_2	49.1	55.1	60.0	30.4	n.d.	0.71	98.3	<0.04	0.54	S	36.7
P_2O_5	n.a.	n.a.	n.a.	n.a.	45.3	41.1	n.a.	n.a.	n.a.	K	<0.02
K_2O	0.10	0.28	3.47	<0.03	0.07	<0.03	0.39	n.d.	<0.01	Ca	<0.05
CaO	10.9	10.2	6.47	0.86	47.1	53.6	0.20	<0.03	0.06	Cr	n.d.
TiO_2	0.44	<0.03	<0.05	0.15	n.d.	0.07	0.17	51.1	23.40	Mn	<0.02
Cr_2O_3	<0.05	<0.01	<0.01	<0.01	n.d.	<0.05	<0.01	n.d.	<0.01	Fe	62.7
MnO	0.77	<0.02	<0.01	1.44	0.10	0.07	<0.01	0.74	0.61	Co	0.13
FeO[b]	27.8	0.55	0.64	63.3	4.8	1.00	0.17	46.9	69.90	Ni	<0.03
Ce_2O_3	n.a.	n.a.	n.a.	n.a.	0.10	0.10	n.a.	n.a.	n.a.	Cu	0.15
Total	99.01	97.57	98.66	98.77	99.76	100.92	100.58	99.05	96.53	Zn	<0.02
										Total	99.85
Fo/En/An[c]	25.6	51.0	35.3	6.1							
Fa/Fs/Or[c]	49.9	1.7	20.0	93.3							
Wo/Ab[c]	24.4	47.3	44.7								
Endmember	$En_{3-50}Fs_{26-96}$ Wo_{2-41}	$An_{37-58}Or_{1-7}$ Ab_{41-59}	$An_{24-43}Or_{5-34}$ Ab_{38-57}	$Fo_{4-9}Fa_{91-96}$							$Fe_{0.99}S$

[a]Endmember composition is calculated.
[b]All Fe as FeO.
[c]Average values.
[d]Apatites contain 2.19 wt% Cl, 1.01 wt% F, and 0.72 wt% H_2O on average as calculated based on stoichiometry; F and Cl has been analyzed using EPMA, 4 nA, 15 kV and 10 μm defocused beam.
Amorph. Fsp = amorphous feldspar, n.a. = not analyzed, n.d. = not detected.

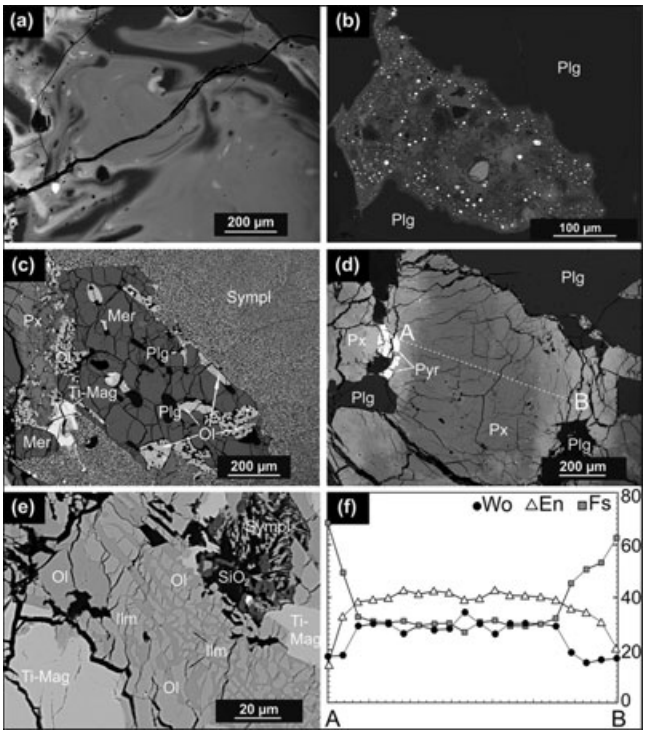

Fig. 5. (a) and (b) shock melt features in KG 002. a) Large patches of glass with schlieren-like texture, feldspathic in composition, are found throughout the sample; light gray = Fe-rich, middle gray = Ca-rich, and dark gray = Al-rich glass, probably reflecting shock melted olivine, pyroxene, and feldspar. b) Shock melt glass containing small FeS droplets (white) and clasts of pyroxene and feldspar enclosed in large plagioclase crystals (Plg). c) Representative merrillite (Mer) grain located at the rim to a fine-grained symplectite (Sympl) patch, which is associated with olivine (Ol), plagioclase (Plg), Ti-magnetite (Ti-Mag), and pyroxene (Px). d) Detailed view of a large pyroxene grain (Px) surrounded by plagioclase (Plg) and pyrrhotite (Pyr), revealing a strong chemical zonation from core to rim, with the composition shown in (f) ranging from Fe-enriched rims to Mg-rich pigeonite core, accompanied by Ca-enrichment toward the core. e) Typical intergrowth of olivine (Ol) with ilmenite (Ilm) in paragenesis with a silica phase (SiO_2), symplectite (Sympl), and Ti-magnetite (Ti-Mag). Except for (f), all images are backscattered electron (BSE) images.

Shock Effects

Ksar Ghilane 002 is heavily shocked, equivalent to an S5 stage, when applying the classification scheme for ordinary chondrites (Stöffler et al. 1991; Bischoff and Stöffler 1992). Evidence for such high shock includes the mosaic extinction of pyroxenes (Fig. 3c), the occurrence of maskelynite (produced by shock transformation of plagioclase), and localized shock melt glass pockets, some of them containing pyroxene- and plagioclase-normative schlieren (Fig. 5a). Similar shock melt pockets have been previously described in the lherzolitic shergottite NWA 1950 (Walton and Herd 2007) and in the shergottite EETA79001 (Fritz et al. 2005; Walton et al. 2010). Fritz et al. (2005) determined a shock pressure of 39 ± 4 GPa for lithology A of EETA79001.

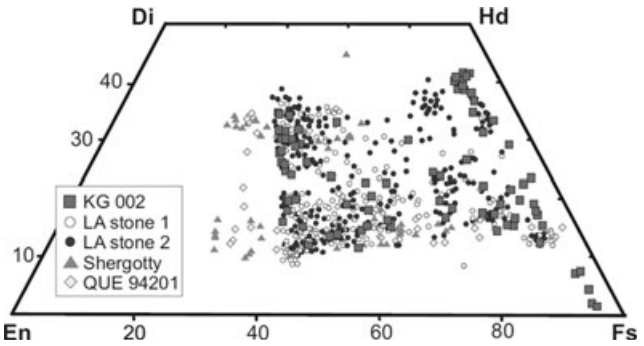

Fig. 6. Ternary phase diagram for the chemical composition of pyroxenes in KG 002. Data are presented relative to other basaltic shergottites, such as Los Angeles (LA), Shergotty, and QUE 94201 (data from Warren et al. 2004). Pyroxene crystals are very heterogeneous in composition. However, they are similar to those described in the Los Angeles shergottite. Only a few pyroxene grains that have been analyzed are more enriched in Fe (see Fs content).

Bulk Chemistry

The bulk composition of KG 002 has been measured for 45 elements. Results for major and minor elements are compiled in Table 2, where two other basaltic shergottites, Los Angeles and Dhofar 378, are included for comparison. It is well known that basaltic shergottites, lherzolitic shergottites, and olivine-phyric shergottites are separable in TiO_2, Al_2O_3, Cr_2O_3, MgO, CaO, and Na_2O abundances (e.g., Shirai and Ebihara 2004). Major element contents of KG 002 fall within the range of basaltic shergottites, in accordance with the petrography and mineral chemistry discussed above. In particular, Al_2O_3 (12.25%), MgO (4.47%), CaO (10.3%), Na_2O (2.14%), and K_2O (0.23%) contents are well within the basaltic shergottite range and far from the other shergottite groups (Lodders 1998). Element abundances (calculated based on EPMA data) are in agreement with ICP data (see Table 2 for comparison). Note that the bulk rock chemical compositions of KG 002, Los Angeles, and Dhofar 378 overlap within uncertainties (Table 2), which suggests a possible genetic relationship. Figure 7 is a plot of Ca/Si versus Mg/Si ratios for Martian meteorites (where the positions of the various shergottite subclasses are indicated). The shergottites spread along a line with endmembers of high Ca/Si and low Mg/Si ratios versus low Ca/Si and high Mg/Si ratios. As clearly confirmed in Fig. 7, KG 002 belongs to the group of basaltic shergottites and represents the most extreme case on the highly evolved

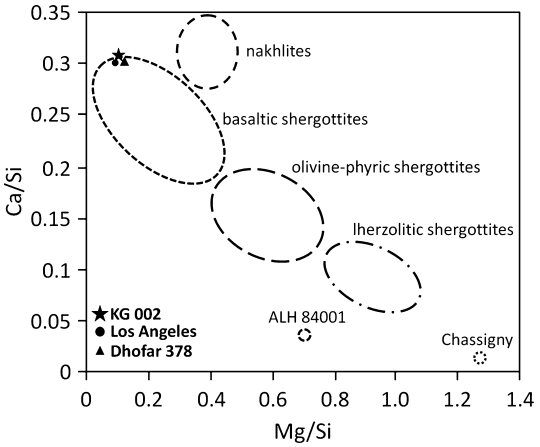

Fig. 7. Plot of Mg/Si versus Ca/Si (atomic ratios) for Martian meteorites showing the position of KG 002.

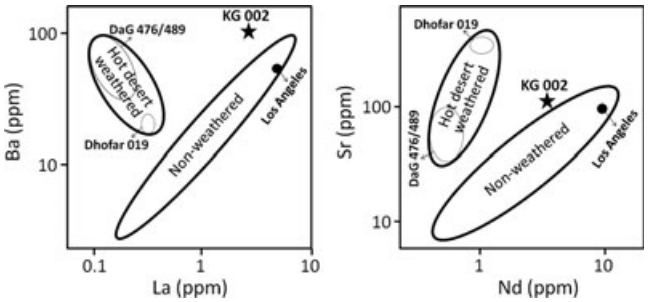

Fig. 8. Concentrations of Ba and Sr versus La and Nd in weathered and nonweathered shergottites (Jambon et al. 2002) showing the position of KG 002.

high Ca/Si, low Mg/Si side. According to the scheme proposed by Irving (2011), and based on its CaO content, Mg/(Mg+Fe), and bulk rock REE pattern (see below), KG 002 belongs to the group of enriched mafic, diabasic shergottites. Other members of this group are, among others, Shergotty, Zagami, Los Angeles, and Dho 378.

Trace element abundances of KG 002 are compiled in Table 4, together with those of Los Angeles for comparison. Concerning alteration, hot desert meteorites often display strong K, Ba, Sr, Cs, U, and Ce enrichments (e.g., Barrat et al. 1999; Stelzner et al. 1999; Zipfel et al. 2000). The Th/U ratio of KG 002 is 3.4, which is in the lower range of values reported for Martian meteorite falls (Th/U ratios of about 3.6–4.3). However, a number of shergottites from hot deserts have even lower Th/U ratios (McLennan 2003). The K/La ratio of KG 002 is 886, which is within the range for most shergottite falls (approximately 700–1000) and distinct from heavily weathered shergottites, which show K/La ratios up to 2000. By comparison, Ba and Sr abundances in KG 002 are only slightly outside the trend defined by nonweathered shergottites in Ba versus La and Sr versus Nd plots, respectively (Fig. 8), but distinct from strongly weathered shergottites in hot deserts, like DaG 476, DaG 489, and Dhofar 019 (Jambon et al. 2002). We therefore conclude that KG 002 is only moderately weathered.

The compatible trace element abundances (such as Ni, Co, Cr, and Cu) of KG 002 are strikingly similar to those reported for Los Angeles (Table 4), which in turn are distinct from other basaltic shergottites (Lodders 1998), thus providing additional evidence for their strong affinity. The REE pattern of KG 002 (Fig. 9) exhibits a pattern similar to Los Angeles and other slightly depleted LREE shergottites including the less evolved Zagami and Shergotty. The positive Ce anomaly (Ce/Ce* ~ 1.2) is probably related to terrestrial weathering, in accordance with the moderate U, Ba, and Sr enrichments discussed above. This anomaly is

Table 4. Trace element abundances (in μg g^{-1}) of KG 002 obtained by ICP-MS. Data for Los Angeles are included for comparison (Jambon et al. 2002).

	KG 002	Los Angeles
Li	7.30 ± 0.06	5.03
Sc	37.9 ± 0.5	41.3
V	201 ± 0.9	–
Co	30.4 ± 0.1	29.2
Ni	32.2 ± 0.2	32.0
Cu	22.1 ± 0.4	22.6
Zn	89.2 ± 0.5	62.3
Rb	7.51 ± 0.07	12.0
Sr	108.7 ± 0.2	81.0
Y	17.0 ± 0.1	29.4
Zr	152 ± 2	79.6
Nb	3.47 ± 0.03	4.99
Mo	0.26 ± 0.02	–
Cd	0.05 ± 0.01	–
Ba	112 ± 1	46.8
La	2.11 ± 0.01	3.97
Ce	6.31 ± 0.04	9.84
Pr	0.74 ± 0.01	1.43
Nd	3.66 ± 0.01	7.07
Sm	1.37 ± 0.01	2.64
Eu	0.76 ± 0.01	1.02
Gd	2.13 ± 0.01	4.28
Tb	0.44 ± 0.01	0.79
Dy	2.91 ± 0.01	5.04
Ho	0.60 ± 0.01	1.03
Er	1.77 ± 0.02	2.76
Tm	0.25 ± 0.01	–
Yb	1.68 ± 0.01	2.35
Lu	0.24 ± 0.01	0.33
Hf	4.57 ± 0.01	2.19
Pb	1.39 ± 0.01	1.12
Th	0.54 ± 0.01	0.57
U	0.16 ± 0.01	0.12

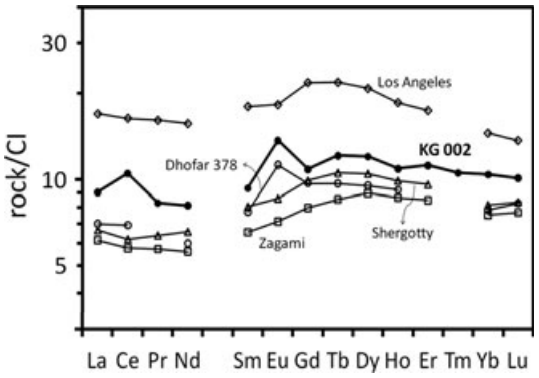

Fig 9. REE pattern of KG 002 compared with Zagami (Barrat et al. 2001), Shergotty (Barrat et al. 2001), Los Angeles (Jambon et al. 2002), and Dhofar 378 (Dreibus et al. 2002).

very rare among Martian meteorites, but has been observed e.g., in the strongly weathered Dhofar 019 shergottite (Neal et al. 2001; Taylor et al. 2002). Ce anomalies are also found in Antarctic shergottites, such as QUE 94201, EETA 79001, and ALHA 77005, and are thought to result from the partial oxidation of Ce^{3+} to Ce^{4+}, where Ce^{4+} is relatively insoluble compared with the rest of the trivalent REE and is less mobile than the other REE during terrestrial weathering (Crozaz et al. 2003). In addition, the REE pattern of KG 002 is characterized by a pronounced positive Eu anomaly (Eu/Eu* ~ 1.4), similar to the basaltic shergottite Dhofar 378, but in contrast to the highly evolved Los Angeles shergottite (Fig. 9), providing additional evidence for complex magma genesis and mantle processes on Mars.

Oxygen Isotopes

Two aliquots of KG 002 were analyzed, yielding $\delta^{18}O$ values of +5.06‰ and +5.23‰. The corresponding $\delta^{17}O$ values were +2.91‰ and +3.14‰. The $\Delta^{17}O$ values were +0.25‰ and +0.40‰ with a mean of +0.32‰, identical within uncertainty. This value falls in the field typical for Martian meteorites (Clayton 1993; Franchi et al. 1999) (Fig. 10).

Noble Gas Analysis

Noble gas results for KG 002 are summarized in Tables 5 and 6, where they are compared with literature data for Los Angeles. Noble gas data for NWA 2800 are not available at this time in the literature. Whilst low concentrations of He and roughly half the Ne budget are released in the 1800 °C step, release of the heavier noble gases Ar, Kr, and Xe occurs preferentially at this temperature (Table 5).

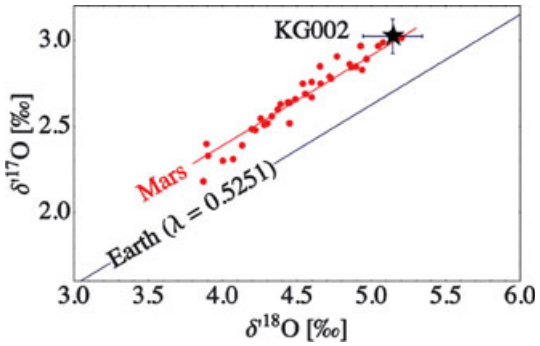

Fig. 10. Plot of $\delta^{17}O$ versus $\delta^{18}O$ showing the data points of two samples from KG 002. The analyses fall within the field of Martian meteorites (Clayton 1993).

Overall, KG 002 shows low He concentrations of ^3He approximately 3×10^{-8} ccSTP/g and ^4He approximately 2×10^{-7} ccSTP g^{-1} compared with previous analyses of Martian shergottites, where the majority show a range of ^3He of 1–7 $\times 10^{-8}$ ccSTP g^{-1} and ^4He 2×10^{-7} to 3×10^{-6} ccSTP g^{-1} (see refs. in Fig. 11 (Ne) for previous shergottite noble gas data). Whereas ^3He is mainly cosmogenic in origin (and thus relates to the CRE age), ^4He concentrations reflect both cosmogenic and radiogenic sources. If we assume a range of cosmogenic $(^4He/^3He)_c$ ratios from 4.0 to 6.0 (Alexeev 1998; Schwenzer et al. 2008), and subtract the associated "cosmogenic" from the measured ^4He, the corrected "radiogenic" ^4He ranges from approximately 3 to 9×10^{-8} ccSTP g^{-1}. Using the U and Th concentrations from Table 4, we can calculate an apparent "crystallization" age range of 0.7–2.5 Ma. This range is close to the calculated CRE age (see below) and hence consistent with essentially complete loss of radiogenic He accumulated at the time of ejection. Radiogenic He loss is a common occurrence in many Martian meteorites (e.g., Schwenzer et al. 2008), and probably relates to shock metamorphism—(see discussion in the Petrography and Mineral Chemistry section).

For Ne, the ^{22}Ne concentration of 8×10^{-9} ccSTP g^{-1} is within the range observed in previous studies of shergottites of approximately 1–13 $\times 10^{-9}$ ccSTP g^{-1} (see refs. in Fig. 11 for previous shergottite data). Figure 11 is a three isotope plot of $^{20}Ne/^{22}Ne$ versus $^{21}Ne/^{22}Ne$ with our step-wise heating data for KG 002, alongside shergottite literature data and various endmember components including "trapped" components Earth's atmosphere (EA), Martian atmosphere (MA), solar wind (SW), as well as cosmogenic neon produced by galactic cosmic rays (GCR), by low-energy solar flare protons (solar cosmic rays, SCR), and cosmogenic Ne produced from sodium (Na) (for associated references, see Fig. 11). Our

Table 5. Noble gas concentrations for KG 002. Previous data reported for the Los Angeles shergottite are also shown. Concentrations are: $^{3-4}$He, ^{40}Ar in 10^{-8} ccSTP g^{-}, $^{20-22}$Ne and $^{36-38}$Ar in 10^{-10} ccSTP g^{-1}, ^{84}Kr and ^{132}Xe in 10^{-12} ccSTP g^{-1}.

	^{3}He	^{4}He	^{22}Ne	^{20}Ne$_t$	^{21}Ne$_c$	^{40}Ar	^{36}Ar$_t$	^{38}Ar$_c$	^{84}Kr	^{80}Kr$_n$	^{83}Kr$_c$	^{132}Xe
KG 002, Bulk sample, 67.53 mg												
600	0.53 ± 0.02	3.35 ± 0.19	4.85 ± 0.14	10.21 ± 0.85	2.64 ± 0.09	9.95 ± 1.01	3.45 ± 0.35	0.06 ± 0.04	2.92 ± 0.30	0.58 ± 0.07	0.13 ± 0.06	1.25 ± 0.37
1000	2.54 ± 0.10	15.44 ± 0.81	37.20 ± 0.99	0.25 ± 1.50	26.60 ± 0.76	16.05 ± 1.62	1.84 ± 0.19	1.36 ± 0.14	6.17 ± 0.40	0.00 ± 0.06	0.04 ± 0.08	1.35 ± 0.37
1800	0.089 ± 0.004	2.70 ± 0.22	36.25 ± 0.96	0.04 ± 1.38	31.23 ± 0.89	196.66 ± 19.68	7.28 ± 1.51	47.67 ± 4.88	29.73 ± 1.58	0.43 ± 0.18	2.44 ± 0.24	27.20 ± 0.81
Sum	3.16 ± 0.10	21.49 ± 0.86	78.30 ± 1. 39	10.50 ± 2.21	60.46 ± 1.17	222.65 ± 19.77	12.57 ± 1.56	49.10 ± 4.89	38.82 ± 1.66	1.01 ± 0.20	2.61 ± 0.26	29.80 ± 0.97
Los Angeles												
	1.69 ± 0.10[a]	21.80 ± 0.70[a]	94.30 ± 6.10[a]	78 ± 7[a]	66 ± 3[a]	386 ± 10[a]	63 ± 5[a]	49.8 ± 3.0[a]	–	0.93 ± 0.40[c]	3.01 ± 0.50[c]	–
	2.64 ± 0.15[b]	29.50 ± 1.00[b]	82.24 ± 4.61[b]	62 ± 5[b]	59 ± 2[b]	340 ± 8[b]	30 ± 4[b]	50.1 ± 2.5[b]	–	–	–	–
	–	–	–	–	–	–	–	–	75[d]	–	–	8.1[d]
	3.14[e]	69.70[e]	86.2[e]	97.9[f]	59.2[f]	298.0[e]	31.7(33.0)[g]	45.1(43.0)[g]	80.4[e]	–	–	29.0[e]

[a]Los Angeles "Bulk 1"; Eugster et al. (2002).
[b]Los Angeles "Bulk 2"; Eugster et al. (2002).
[c]Eugster et al. (2002).
[d]Busemann and Eugster (2002).
[e]Garrison and Bogard (2000).
[f]Calculated from (Garrison and Bogard 2000).
[g]Trapped components with assumed EA (and MA).
t = trapped, c = cosmogenic. For component correction, see text.

Table 6. Isotopic and elemental noble gas ratios for KG 002, previous data for Los Angeles and endmember components.

	$^{3}He/^{4}He$	$^{20}Ne/^{22}Ne$	$^{21}Ne/^{22}Ne$	$(^{22}Ne/^{21}Ne)_c$	$^{38}Ar/^{36}Ar$	$^{40}Ar/^{36}Ar$	$^{129}Xe/^{132}Xe$	$(^{36}Ar/^{132}Xe)_t$	$(^{84}Kr/^{132}Xe)_t$
KG 002, Bulk sample, 67.53 mg									
600	0.158 ± 0.009	2.757 ± 0.042	0.550 ± 0.008	1.443 ± 0.027	0.204 ± 0.010	308.5 ± 13.0	1.017 ± 0.091	280.3 ± 87.9	2.320 ± 0.731
1000	0.164 ± 0.008	0.836 ± 0.009	0.715 ± 0.007	1.398 ± 0.015	0.627 ± 0.017	619.5 ± 17.9	1.014 ± 0.081	137.8 ± 40.5	4.606 ± 1.301
1800	0.033 ± 0.003	0.831 ± 0.010	0.861 ± 0.009	1.161 ± 0.012	1.282 ± 0.027	514.5 ± 5.5	1.033 ± 0.012	26.8 ± 5.6	1.058 ± 0.066
Sum	0.147 ± 0.006	0.953 ± 0.008	0.773 ± 0.005	1.277 ± 0.009	1.157 ± 0.026	504.8 ± 5.1	1.032 ± 0.012	42.4 ± 5.5	1.270 ± 0.069
Los Angeles									
	0.078 ± 0.004[a]	1.58 ± 0.08[a]	0.690 ± 0.038[a]	1.35 ± 0.07[a]	0.60 ± 0.04[a]	405 ± 19[a]	–	–	–
	0.090 ± 0.004[b]	1.52 ± 0.07[b]	0.704 ± 0.030[b]	1.33 ± 0.06[b]	0.89 ± 0.03[b]	545 ± 20[b]	–	–	–
	–	–	–	–	–	–	1.140 ± 0.030[c]	650 ± 75[c]	9.3 ± 1.3[c]
	0.05[d]	1.87[d]	0.69[d]	1.288 ± 0.005	0.84[d]	489[d]	1.103[d]	–	–
Endmember components									
EA	–	9.800 ± 0.080[e]	0.0290 ± 0.0003[e]	–	0.1885 ± 0.0003[f]	298.6 ± 0.3[f]	0.9832 ± 0.0012[g]	1347[h]	27.8[h]
EFA	–	–	–	–	–	–	0.9832 ± 0.0012[gi]	25 ± 5[j]	1.2 ± 0.24[i]
MA	–	10.1 ± 0.7[k]	0.03 ± 0.01[l]	–	0.244 ± 0.012[l]	3000 ± 500[m]	2.40 ± 0.02[p]	431.4 ± 122.0[q]	11.1 ± 3.1[q]
MI	–	–	–	–	–	–	1.029 ± 0.019[r]	9.21 ± 7.28[r]	1.14 ± 0.12[r]
	"Chass-S"		–	–	0.245 ± 0.006[s]	1860 ± 48[s]	1.081 ± 0.004[s]	<5[s]	<1.10[s]
	"Chass-E"		–	–	1.127 ± 0.028[t]	1023 ± 28[t]	<1.07[t]	>130[t]	>1.8[t]

[a]Los Angeles "Bulk 1"; Eugster et al. (2002).
[b]Los Angeles "Bulk 2"; Eugster et al. (2002).
[c]Busemann and Eugster (2002).
[d]Garrison and Bogard (2000).
[e]Eberhardt et al. (1965).
[f]Lee et al. (2006).
[g]Basford et al. (1973).
[h]Pepin (1991); Swindle (2002).
[i]Mohapatra et al. (2002).
[j]Mohapatra et al. (2009).
[k]Calculated average from Swindle et al. (1986); Wiens et al. (1986).
[l]Assumed; Wiens et al. (1986).
[m]Owen et al. (1977).
[p]SPB-Xe ; Swindle et al. (1986).
[q]Swindle et al. (1986); Pepin (1991).
[r]Chassigny PB4 1600 °C; Ott (1988).
[s]Chassigny-Ol 500 °C; Mathew and Marti (2001).
[t]Chassigny-Ol > 1040 steps; Mathew and Marti (2001).
t = trapped, c = cosmogenic. For component correction, see text.

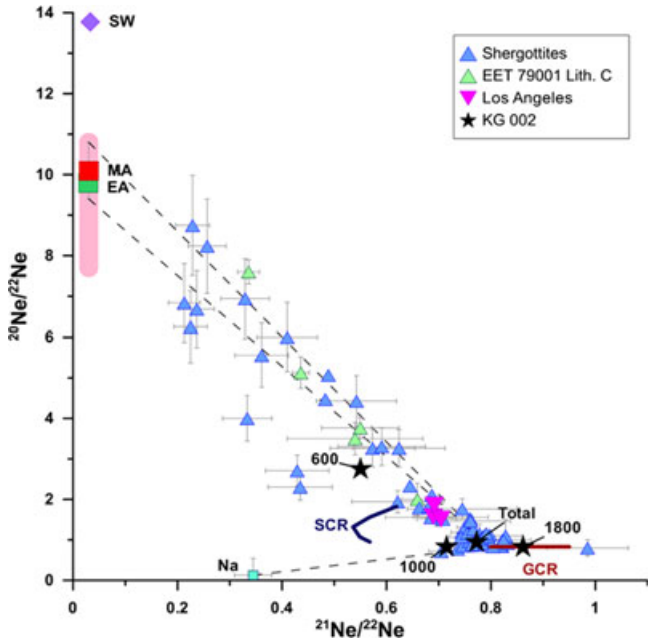

Fig. 11. Three isotope plot of $^{21}Ne/^{22}Ne$ versus $^{20}Ne/^{22}Ne$ showing the step-heated results for KG 002. Other components plotted include SW (Heber et al. 2009), MA (Swindle et al. 1986; Wiens et al. 1986), EA (Eberhardt et al. 1965), GCR (Garrison et al. 1995), SCR (0.5–10 g cm^{-2}, R_0 = 70 MV; Reedy 1992), contribution from Na (Smith and Huneke 1975). Also shown for comparison are previous data for shergottites (including EET 79001 lithology C) (Becker and Pepin 1984, 1986; Bogard et al. 1984; Swindle et al. 1986; Wiens et al. 1986; Ott 1988; Wiens 1988; Eugster et al. 1997; Garrison and Bogard 1998; Mathew et al. 2003; Schwenzer et al. 2007; Mohapatra et al. 2009) and Los Angeles (Garrison and Bogard 2000; Eugster et al. 2002). The thick pink line depicts the range of Ne ratios for MA reported in previous data (Swindle et al. 1986; Wiens et al. 1986; Ott and Löhr 1992). The dashed lines represent mixing between GCR and upper/lower limits on MA, or GCR and Na. KG 002 plots within the range observed for previous analyses of shergottites, and shows evidence for slight SCR and Na interaction.

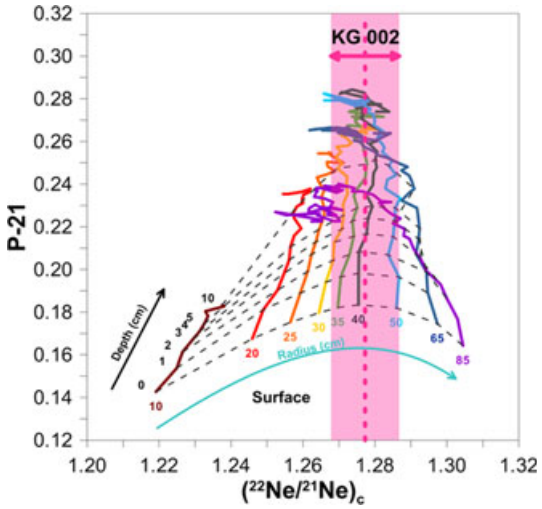

Fig. 12. A plot of the cosmogenic ^{21}Ne production rate P-21 (10^{-8} ccSTP g^{-1}/Ma^{-1}) versus cosmogenic $(^{22}Ne/^{21}Ne)_c$ based on the Monte Carlo model by Leya and Masarik (2009) and an average major element abundance for KG 002 from Table 2, and the trace element abundances from Table 4. The colored full lines represent different potential pre-atmospheric radii for the meteorite (in cm), whilst the dashed black lines represent the depth within a sample of such radius (in cm). The pink band represents the total measured $(^{22}Ne/^{21}Ne)_c$ for KG 002 (Table 6). It is clear that with the cosmogenic $(^{22}Ne/^{21}Ne)_c$ ratio of 1.277 ± 0.009, a preatmospheric radius of ≤ 25 cm can be excluded.

KG 002 results plot within the range observed in previous shergottite analyses and indicate contributions from GCR, Na, and possibly mixing with a minor amount of SCR, as well as mixing with an atmospheric component. As the most significant shift toward terrestrial atmosphere is observed in the lowest temperature step (600 °C), this may very well represent mixing with terrestrial air due to contamination, rather than Martian atmosphere (Fig. 11). The cosmogenic $(^{21}Ne/^{22}Ne)_c$ ratio for the sample is 0.783 ± 0.006, consistent with the range observed in previously studied Martian meteorites. Whilst it has been suggested that such ratios require contribution from SCR-Ne, comparison with GCR-Ne production rates based on Leya and Masarik (2009) and the chemical composition of KG 002 (Tables 2 and 4) shows that for KG 002—while a small presence cannot be excluded—SCR-Ne is not required (see Fig. 12). This is because of the extremely low abundance of Mg and the high abundance of Na (approximately 1.8%), contributing Ne with extremely low $^{21}Ne/^{22}Ne$ (Fig. 11). For example, the $(^{22}Ne/^{21}Ne)_c$ ratio modeled for KG 002 using Leya and Masarik (2009) production rates shows a significant 0.10 reduction if Na is omitted. Furthermore, the 1000 °C temperature step plots right on the mixing trend from common GCR to Na spallation, with no evidence for enhanced $^{20}Ne/^{22}Ne$ as seen in SCR produced Ne.

For the heavier noble gases, it is difficult to distinguish between separate components within KG 002 when relying solely on isotopic ratios. For example, the $^{129}Xe/^{132}Xe$ ratio may indicate mixing between major components of Martian atmosphere and/or Martian interior and/or Earth's atmosphere (Table 6). Combining this with the heavy noble gas elemental ratios may provide a better insight. Figure 13 is a plot of $^{129}Xe/^{132}Xe$ ratios versus elemental ratios of trapped $^{36}Ar_t/^{132}Xe$ and $^{84}Kr/^{132}Xe$, including shergottite literature data, Earth's atmosphere (EA), elementally fractionated atmosphere (EFA), Martian atmosphere (MA), Martian interior (MI), and further distinct

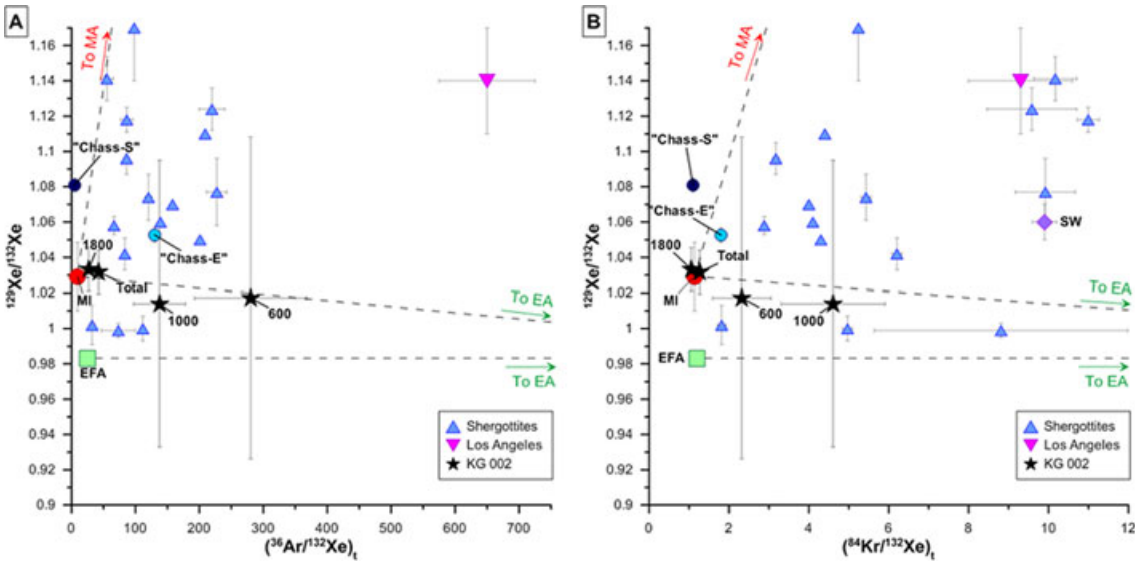

Fig. 13. Plots of $^{129}Xe/^{132}Xe$ versus A) $(^{36}Ar/^{132}Xe)_t$ and B) $(^{84}Kr/^{132}Xe)_t$ for our step-heated KG 002 data. Other components plotted include SW (Vogel et al. 2011), EA (Basford et al. 1973; Pepin 1991; Swindle 2002), EFA (Mohapatra et al. 2002, 2009), MA (Swindle et al. 1986; Pepin 1991), MI (Ott 1988), and further interior components "Chass-S" and "Chass-E" (Mathew and Marti 2001). Previous data for shergottites (Mathew et al. 2003; Mohapatra et al. 2009) and Los Angeles (Busemann and Eugster 2002) are shown for comparison. Mixing between EA, MA, MI and EA and EFA are shown as dashed lines. The high temperature 1800 °C KG 002 step shows strong similarities with MI, whilst the lower temperature 600 and 1000 °C steps had low concentrations of gas and show some influence from EA and/or EFA.

interior components "Chass-S" and "Chass-E" (for associated references, see Fig. 13; Table 6 captions). This plot indicates that Martian interior may be a dominant noble gas component in KG 002, which is highlighted in the 1800 °C release (Fig. 13). Alternatively, we may have identified an additional distinct interior component with an elevated $^{40}Ar/^{36}Ar$ ratio and $^{129}Xe/^{132}Xe$ identical to the Martian interior 1.029 ± 0.019 as defined by Ott (1988), which was also released at the highest temperature step. It is difficult to assess the effect of EFA on observed ratios, especially as the releases for 600 and 1000 °C have low amounts of gas and therefore large analytical uncertainties (Fig. 13).

Cosmic Ray Exposure Ages

Cosmic ray exposure (CRE) ages for Martian meteorites found in the literature have commonly been calculated using the empirical $^{22}Ne/^{21}Ne$-corrected production rate equations of Eugster and Michel (1995). Using this approach and assuming that KG 002 is a basaltic shergottite (and thus has production systematics similar to that of eucrites [Eugster et al. 1997]), combined with an average of the major element abundances given in Table 2 for KG 002, the trace element data in Table 4, and the cosmogenic concentrations given in Table 5, we obtain T_3 (^3He), T_{21} (^{21}Ne), and T_{38} (^{38}Ar), ages of 1.97 ± 0.06, 4.42 ± 0.11, and 2.90 ± 0.29 Ma, respectively. Whilst the ^3He concentration was assumed to be entirely cosmogenic, the T_{21} age was calculated from the cosmogenic $^{21}Ne_c$ concentration, as obtained assuming the trapped component to have EA composition (Eberhardt et al. 1965) and the cosmogenic component to have a typical GCR $^{20}Ne/^{22}Ne$ ratio (0.83, e.g., Garrison et al. 1995). The T_{38} age was calculated from the cosmogenic $^{38}Ar_c$ concentration, assuming a trapped component with the $^{38}Ar/^{36}Ar$ ratio of EA (Lee et al. 2006), and a cosmogenic $(^{38}Ar/^{36}Ar)_c$ ratio of approximately 1.5 (Wieler 2002). Note that the errors include uncertainties related to the concentrations of cosmogenic gas as well as the shielding parameter, but not such related to chemical composition. The nominal ages given above show a large scatter. However, it is important to note that the determination of CRE ages for meteorites with unusual chemical compositions is not straightforward. In fact, using the shielding-dependent production rates from Leya and Masarik (2009) and neglecting any possible SCR contribution (minor, if anything, as discussed above), we obtain about 30% shorter CRE ages. This is discussed in more detail below, in the context of comparison with the shergottite Los Angeles and the radionuclide data.

Kr isotopes were partitioned into trapped, cosmogenic, and neutron capture components, using a trapped $^{83}Kr/^{84}Kr$ ratio of 0.2025 ± 0.0025 and a cosmogenic composition derived from an analysis of

eucrite Stannern (Bogard et al. 1971). A rather large meteoroid size is indicated by the presence of excess ^{80}Kr of neutron capture origin ($^{80}Kr_n$). The concentration of $1.01 \pm 0.20 \times 10^{-12}$ mL g^{-1} (Table 5) is at the high end of what has previously been observed for Martian meteorites (Eugster et al. 2002), including Los Angeles ($0.93 \pm 0.40 \times 10^{-12}$ mL g^{-1}). Unfortunately, we do not have data for the Br concentration, so it is not possible to deduce a neutron fluence at this time.

Crystallization Age

For the crystallization age, we can calculate a nominal K-Ar age of 279 ± 27 Ma based on the total ^{40}Ar and K concentrations in the meteorite, assuming that all ^{40}Ar is radiogenic (Tables 2 and 5). However, many Ar-Ar ages calculated for shergottites are older compared with other chronometers—a feature which has been ascribed to excess ^{40}Ar (e.g., Bogard et al. 2009). By assuming that all trapped ^{36}Ar is related to trapped EA (i.e., subtraction of the equivalent ^{40}Ar), we can calculate a K-Ar age of 119 ± 30 Ma. As detailed above, an U-Th-He age for this meteorite is not viable due to the low He concentrations probably caused by He loss during shock metamorphism.

Comparison with Los Angeles

The available data for Los Angeles (Garrison and Bogard 2000; Busemann and Eugster 2002; Eugster et al. 2002) are also displayed in Tables 5 and 6, along with the KG 002 results. For NWA 2800, there are no noble gas data in the literature at this time. There is remarkable similarity between KG 002 and Los Angeles in the concentrations of cosmogenic Ne and Ar (including $(^{22}Ne/^{21}Ne)_c$ ratios). However, the situation is different for trapped Ne and Ar ($^{20}Ne_t$, $^{36}Ar_t$), as well as for ^{40}Ar and ^{84}Kr, where abundances for KG 002 are lower compared with all Los Angeles data (Table 5). For ^4He, KG 002 is similar to Los Angeles bulk 1 and 2 reported by Eugster et al. (2002) (approximately 2×10^{-7} ccSTP g^{-1}), but significantly lower than the ^4He concentration reported by Garrison and Bogard (2000) (approximately 7×10^{-7} ccSTP g^{-1}). Finally, the KG 002 ^{132}Xe concentration is similar to that reported for Los Angeles by Garrison and Bogard (2000) (approximately 3×10^{-11} ccSTP g^{-1}), but significantly higher than that reported by Busemann and Eugster (2002) (approximately 8×10^{-12} ccSTP g^{-1}). In addition, Los Angeles may show more influence from both the Martian and terrestrial atmosphere compared with KG 002, with an elevated $^{129}Xe/^{132}Xe$ ratio of approximately 1.14, $^{36}Ar_t/^{132}Xe$ of approximately 650, and $^{84}Kr/^{132}Xe$ ratio of approximately 9.3 (Busemann and Eugster 2002) compared with approximately 1.03, 42, and 1.3, respectively (Table 6; Fig. 13).

A number of crystallization ages have been calculated for Los Angeles, including an Rb-Sr age of 165 ± 11 Ma (Nyquist et al. 2000), Sm-Nd ages of 172 ± 8, and 181 ± 13 Ma (Nyquist et al. 2001; Bouvier et al. 2008), a Lu-Hf age of 159 ± 42 Ma (Bouvier et al. 2008), and an older Pb-Pb age of 4050 ± 70 Ma (Bouvier et al. 2008). Whilst the young ages for Los Angeles (and other shergottites) may result from resetting by shock or be due to the presence of phosphates (Bouvier et al. 2005, 2008), the upper and apparent lower limits on the K-Ar age for KG 002 age of approximately 120 and 280 Ma provide no strong evidence for a true age difference. Thus, both meteorites may have experienced similar resetting events or conditions.

In terms of determining the possibility of a "launch pairing" for Los Angeles and KG 002 based on the noble gas CRE ages, assessing a correlation is not straightforward. Preferred CRE ages for Los Angeles have been reported based on T_{81} (^{81}Kr) of 3.10 ± 0.70 and 3.35 ± 0.30 Ma (Terribilini et al. 2000; Eugster et al. 2002). These are similar to our T_{38} age of 2.9 Ma. Eugster et al. (2002) and Garrison and Bogard (2000) also report T_3, T_{21}, and T_{38} ages for Los Angeles of approximately 1.35–1.9, 3.13–3.6, and 3.23–2.8 Ma, respectively, which cover the same range. The T_3 ages are low compared with the T_{21} and T_{38} ages, a feature also observed for our KG 002 analysis. Concerning ^{21}Ne, it is important to note that Garrison and Bogard (2000) corrected their $^{21}Ne_c$ concentration for production from Na and then, based on this corrected value, calculated a T_{21} of 3.6 Ma using the $(^{22}Ne/^{21}Ne)_c$ ratio of approximately 1.163 from their highest temperature release (1600 °C), as this temperature step should be the least affected by production on Na. Eugster et al. (2002) followed the same approach, arriving at a T_{21} age of 3.15 Ma. If we perform a similar correction on our total $^{21}Ne_c$ concentration based on a 4.4% Na contribution to $^{21}Ne_c$ (estimated from the Na content given in Table 2 and "typical" production rates on sodium [Leya and Masarik 2009]) and only use our 1800 °C temperature step for the $(^{22}Ne/^{21}Ne)_c$ shielding parameter (1.161 ± 0.012, compared to 1.277 ± 0.009 from the total release), we obtain a T_{21} age of 3.44 ± 0.11 Ma. This value is in agreement with the (presumably more reliable) T_{38} age of 2.90 ± 0.29 Ma.

In summary, although the noble gas concentrations and ratios for Los Angeles and KG 002 are somewhat different, the crystallization age data may hint at similar resetting events. More importantly, the CRE ages of both meteorites show a strong resemblance. Based on

the production rate systematics of Eugster et al. (2002), an ejection event approximately 3.0 Ma ago is suggested.

Shielding Conditions and CRE Ages from Cosmogenic Radionuclides and the Physical Model of Leya and Masarik (2009)

Cosmogenic radionuclide data of KG 002 in comparison with earlier published ones for Los Angeles are summarized in Table 7. The given uncertainties include AMS measurement uncertainties (statistical and from used calibration materials), but none from stable isotope detection (^{26}Al and ^{55}Mn) nor Fe-measurements for normalizing purposes of ^{53}Mn. The measured ^{60}Fe/Fe of KG 002 is 6.2×10^{-16} ($+2 \times 10^{-15}$; -1.5×10^{-17}) and was not further interpreted due to the large uncertainty associated with the experimental value. Data given by Nishiizumi et al. (2000) and Berezhnoy et al. (2010) for Los Angeles mostly agree well with ^{10}Be and ^{53}Mn data of KG 002, whereas the higher ^{26}Al activity of KG 002, in comparison with Los Angeles, originates partially from the high abundance of stable Al, accounting for about one third of the total ^{26}Al production in KG 002 according to Monte Carlo-based depth- and radius-dependent production rates (Leya and Masarik 2009). In fact, the ^{26}Al value of (116.1 ± 1.9) dpm kg^{-1}, being the highest value ever measured in a Martian meteorite, can be explained solely by GCR-induced production.

When comparing the cosmogenic radio- and stable nuclides with the above-mentioned Monte Carlo calculations, an irradiation history for KG 002 can be reconstructed step by step:

1. The cosmogenic ^{22}Ne/^{21}Ne being 1.277 ± 0.009 excludes pre-atmospheric radii $\leq$ 25 cm (Fig. 12).
2. Calculated saturation activities of ^{10}Be and ^{26}Al cannot be brought into any overlap with experimental values of KG 002, thus pointing to a shorter CRE than necessary for saturation of ^{10}Be (Fig. 14, upper left). Taking into consideration the CRE age from ^{38}Ar determination and the empirical approach, 2.9 Ma, the ^{26}Al activity is near the saturation level (94.2%), whereas ^{10}Be is undersaturated (Fig. 14, upper right). Generally, CRE ages between 2.8 and 3.7 Ma (Fig. 14, lower left and right) are possible, the lower value asking for a smaller radius (approximately 35–50 cm), the higher values (3.5–3.7 Ma) correspond to a radius of approximately 65 cm. For all scenarios, the investigated sample originates from a position near the center. We note, however, that this scenario may not be unique. An alternative story might involve partial production of ^{26}Al by SCR. However, this would require about 50% of total ^{26}Al being of SCR-origin if comparing $(^{22}Ne/^{21}Ne)_c$ and ^{26}Al production rates, which seems rather unlikely. Note, in this context, also the lack of evidence for significant SCR contribution to neon.
3. Another, also very sensitive, radionuclide for CREs in the 3 Ma region is the one with the longest half-life investigated here, i.e., ^{53}Mn. However, having the highest measurement uncertainty (>20%), mainly due to the difficulties of isobar separation of ^{53}Cr and lack of repeat measurements, the nuclide does not yet allow for constraining the CRE age of KG 002 with higher precision. A reduction in the uncertainty down to the 10% level would exclude the younger ages of the 2.8–3.7 Ma spread.

Table 7. Cosmogenic radionuclide data and corresponding 1 σ-uncertainties for KG 002 (this work).

	^{10}Be (dpm/kg)	^{26}Al (dpm/kg)	^{53}Mn (dpm/kg Fe)
KG 002	18.27 ± 0.35	116.1 ± 1.9	300 ± 64
Los Angeles*			
LA-1 (0–2 mm)	18.4 ± 0.4	95.5 ± 2.4	
LA-1 (1–4 mm)	19.5 ± 0.4	103.0 ± 3.8	
LA-2 (exterior)	18.4 ± 0.3	89.6 ± 3.0	
Los Angeles#	16.8 ± 0.5	77.7 ± 3.7	251 ± 14
	→17.6 ± 0.5 (renorm.)		

Data reported for the Los Angeles shergottite by Nishiizumi et al. (2000) measured at LLNL (marked *) and Berezhnoy et al. (2010) measured at PRIMELab and Munich (marked #) are shown for comparison. To make ^{10}Be data directly comparable, the PRIMELab data have been renormalized by a factor of 1.045 to DREAMS data according to the recently found disparity (Merchel et al. 2012), whereas LLNL ^{10}Be/^{9}Be data are generally only about 0.4% lower than DREAMS data, and thus remain as they were published. This renormalization is based on pure experimental between-lab measurement differences using the same ^{10}Be standard (Merchel et al. 2012).

As the experimental ^{26}Al is near the saturation level, a long terrestrial age influencing the ^{26}Al concentration can be excluded. In essence, from the reasoning above, a simple one-stage irradiation model can explain all three radionuclides and the associated $(^{22}Ne/^{21}Ne)_c$: Ksar Ghilane 002 has been of medium-sized radius (35–65 cm) and travelled 2.8–3.7 Ma through space before entering the Earth's atmosphere. The investigated sample was probably from an effectively shielded position near the center, thus, excluding SCR-induced nuclear reaction products as inferred for other shergottites. In this version, the CRE age of KG 002 from noble gases based on the empirical production rate, and for radionuclides based on the Monte Carlo calculated rates agrees well with the ages calculated for Los Angeles: (3.0 ± 0.4) and 3.3 Ma from ^{10}Be and 2.8–3.1 Ma from several noble

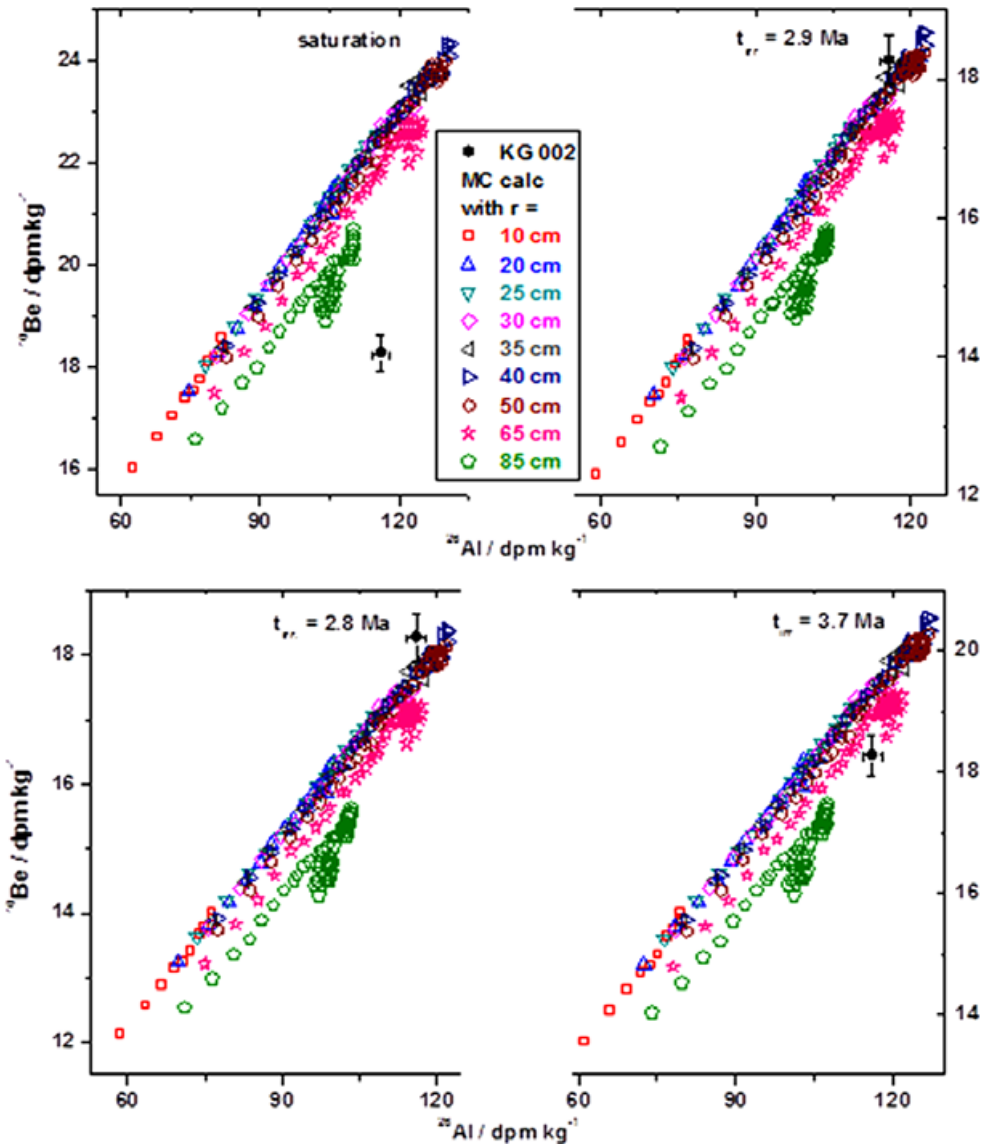

Fig. 14. Experimental ^{10}Be and ^{26}Al concentrations of KG 002 in comparison with Monte Carlo-calculated depth- and radius-dependent production rates for saturation and three different CRE ages (2.8, 2.9, and 3.7 Ma).

gases (Nishiizumi et al. 2000; Terribilini et al. 2000; Berezhnoy et al. 2010). However, the deduced meteoroid radii (20–40 cm), which were originally based on calculations assuming the same chemical composition for Los Angeles as QUE 94201, nearly exclude a common travel in a single meteoroid, asking for individual exposure of both meteoroids after a conjoint ejection event on Mars.

Finally, it is important to realize that significant systematic uncertainties exist in the calculation of cosmic ray exposure ages, in particular for meteorites with unusual chemistry. Surprisingly, whilst we have obtained consistent CRE ages for KG 002 based on the *empirical* approach for noble gases and the *Monte Carlo approach* for radionuclides, we obtain significantly lower CRE ages T_{21} and T_{38} if we consistently use the Monte Carlo approach and the shielding conditions (near the center) implied from the radionuclides: approximately 2.2 Ma (versus approximately 3.0 Ma). In fact, it is virtually impossible to arrive at approximately 3 Ma with realistic shielding conditions in the Monte Carlo model. Notably, the discrepancy holds both for T_{21} and T_{38}, which essentially agree with each other in both approaches. Luckily, in some way, if we extend our approach to the noble gas data published for Los Angeles, we find the situation to be the same. Thus, most important in this context (and in a way that is reassuring), CRE ages for the two meteorites are indistinguishable, whatever the true value may be.

CONCLUSIONS

Ksar Ghilane 002, recovered in January 2010 in Tunisia, has been listed in the Meteoritical Bulletin Database as the 100th Martian meteorite fragment accepted by the Nomenclature Committee.

Based on oxygen isotope data and mineralogical studies, KG 002 is a coarse-grained basaltic shergottite similar to Los Angeles and NWA 2800 and is probably the feldspar (maskelynite)-richest rock among the Martian meteorites. Besides the major phases maskelynite and pyroxene, the rock also contains Fe-rich olivine, the two Ca-phosphates merrillite and Cl-apatite, silica (and/or SiO_2-normative K-rich glass), amorphous K-feldspar, pyrrhotite, Ti-magnetite, ilmenite, and baddeleyite as minor or accessory mineral constituents. A typical feature of KG 002 is the high abundance of symplectitic areas composed of fine-grained intergrowths of fayalite, Ca-pyroxene, and a silica phase, which may have formed by the breakdown of pyroxferroite at low pressure during slow cooling. It should be noted that the symplectites in KG 002 (up to 2 mm in apparent size) are larger than in other Martian meteorites, indicating that the pyroxferroite crystals had to be very large prior to their breakdown.

As observed for most of the shergottites, all plagioclase in KG 002 has been transformed to maskelynite by shock indicating a shock stage of S5. The shock event producing this conversion is probably also responsible for the formation of impact melt patches of variable chemical compositions and He loss in the bulk rock.

Major element concentrations clearly indicate the basaltic composition of the rock. Ksar Ghilane 002 has CaO- and Al_2O_3-concentrations higher than that of other shergottites, such as Los Angeles and Dhofar 378, consistent with the highest modal feldspar abundance among these rocks. Considering the REEs, KG 002 has a similar pattern to that of Los Angeles showing a slight relative depletion of the light REE; however, the concentrations are about a factor of two lower than those in Los Angeles. The small positive Eu anomaly of KG 002 may indicate a complex magma genesis and might be explained by abundant plagioclase accumulation. On the other hand, the small positive Ce anomaly does not appear to be a primordial feature, but rather probably results from terrestrial weathering.

Our noble gas data suggest that gases with a composition inferred to be typical for the Martian interior (possibly mantle, e.g., Ott 1988) dominate the inventory of trapped noble gases. In addition, there may be some influence from elementally fractionated atmosphere. Although KG 002 does not represent a mantle rock, the source region of the magma (carrying the noble gas isotope signature) might thus be within the mantle. Our apparent crystallization ages are within the previously reported range for shergottites (approximately 100–600 Ma), and may result from resetting events. In terms of a comparison with Los Angeles, whilst we have observed differences in gas concentrations and isotopic ratios, the similar apparent crystallization age/resetting event and strong resemblance in CRE ages may provide evidence for a launch-pairing, which may have happened approximately 3.0 Ma ago (for the empirical production rates) or approximately 2.2 Ma (production rates from the Monte Carlo approach). A CRE age of 2.8–3.7 Ma of KG 002 does overlap with the earlier published ages (^{10}Be, noble gases) of Los Angeles. Based on the Monte Carlo approach, the pre-atmospheric radius of KG 002 should have been between 35 and 65 cm with the investigated sample originating from near the center.

Acknowledgments—J. L. is grateful to ICREA Academia program. We thank U. Heitmann (Münster) for sample preparation. The DREAMS accelerator team, in particular S. Akhmadaliev, is gratefully thanked for helping with ^{10}Be and ^{26}Al measurements, and T. Faestermann and G. Korschinek for ^{53}Mn and ^{60}Fe measurements at Munich.

Editorial Handling—Dr. A. J. Timothy Jull

REFERENCES

Akhmadaliev S., Heller R., Hanf D., Rugel G., and Merchel S. 2013. The new 6 MV AMS-facility DREAMS at Dresden. *Nuclear Instruments and Methods in Physics Research B* 294:5–10.

Alexeev V. A. 1998. Parent bodies of L and H chondrites: Times of catastrophic events. *Meteoritics & Planetary Science* 33:145–152.

Aramovich C. J., Herd C. D. K., and Papike J. J. 2002. Symplectites derived from metastable phases in Martian basaltic meteorites. *American Mineralogist* 87:1351–1359.

Armstrong J. T. 1991. Quantitative elemental analysis of individual microparticles with electron beam instruments. *Electron probe quantitation*, edited by Heinrich K. F. J. and Newbury D. E. New York: Plenum Press. pp. 261–315.

Asprey L. B. 1976. The preparation of very pure F_2 gas. *Journal of Fluorine Chemistry* 7:359–361.

Barrat J. A., Gillet P., Lesourd M., Blichert-Toft J., and Popeau G. R. 1999. The Tatahouine diogenite: Mineralogical and chemical effects of sixty-three years of terrestrial residence. *Meteoritics & Planetary Science* 34: 91–97.

Barrat J. A., Blichert-Toft J., Nesbitt R. W., and Keller F. 2001. Bulk chemistry of Saharan shergottite Dar al Gani 476. *Meteoritics & Planetary Science* 36:23–29.

Basford J. R., Dragon J. C., and Pepin R. O. 1973. Krypton and xenon in lunar fines. Proceedings, 4th Lunar Science Conference. pp. 1915–1955.

Becker R. H. and Pepin R. O. 1984. The case for a Martian origin of the shergottites: Nitrogen and noble gases in EETA79001. *Earth and Planetary Science Letters* 69:225–242.

Becker R. H. and Pepin R. O. 1986. Nitrogen and light noble gases in Shergotty. *Geochimica et Cosmochimica Acta* 50:993–1000.

Berezhnoy A. A., Bunch T. E., Ma P., Herzog G. F., Knie K., Rugel G., Faestermann T., and Korschinek G. 2010. Al-26, Be-10, and Mn-53 in Martian meteorites (abstract). *Meteoritics & Planetary Science* 45:A13.

Bischoff A. and Stöffler D. 1992. Shock metamorphism as a fundamental process in the evolution of planetary bodies: Information from meteorites. *European Journal of Mineralogy* 4:707–755.

Bogard D. D., Huneke J. C., Burnett D. S., and Wasserburg G. J. 1971. Xe and Kr analyses of silicate inclusions from iron meteorites. *Geochimica et Cosmochimica Acta* 35: 1231–1254.

Bogard D. D., Nyquist L. E., and Johnson P. 1984. Noble gas contents of shergottites and implications for the Martian origin of SNC meteorites. *Geochimica et Cosmochimica Acta* 48:1723–1739.

Bogard D., Park J., and Garrison D. H. 2009. ^{39}Ar-^{40}Ar "ages" and origin of excess ^{40}Ar in Martian shergottites. *Meteoritics & Planetary Science* 44:905–923.

Bouvier A., Blichert-Toft J., Vervoort J. D., and Albarède F. 2005. The age of SNC meteorites and the antiquity of the Martian surface. *Earth and Planetary Science Letters* 240:221–233.

Bouvier A., Blichert-Toft J., Vervoort J. D., Gillet P., and Albarède F. 2008. The case for old basaltic shergottites. *Earth and Planetary Science Letters* 266:105–124.

Bunch T. E., Irving A. J., Wiitke J. H., and Huehner S. M. 2008. Highly evolved basaltic shergottite Northwest Africa 2800: A clone of Los Angeles (abstract #1953). 39th Lunar and Planetary Science Conference. CD-ROM.

Busemann H. and Eugster O. 2002. The trapped heavy noble gases in recently found Martian meteorites (abstract #1823). 33rd Lunar and Planetary Science Conference. CD-ROM.

Clayton R. N. 1993. Oxygen isotopes in meteorites. *Annual Review of Earth and Planetary Sciences* 21:115–149.

Connolly H. C., Jr., Smith C., Benedix G., Folco L., Righter K., Zipfel J., Yamaguchi A., and Aoudjehane H. C. 2008. The Meteoritical Bulletin, No. 93. *Meteoritics & Planetary Science* 43:571–632.

Crozaz G., Floss C., and Wadhwa M. 2003. Chemical alteration and REE mobilization in meteorites from hot and cold deserts. *Geochimica et Cosmochimica Acta* 67:4727–4741.

Dreibus G., Wlotzka F., Huisl W., Jagoutz E., Kubny A., and Spettel B. 2002. Chemistry and petrology of the most feldspathic shergottite: Dhofar 378 (abstract). *Meteoritics & Planetary Science* 37:A43.

Eberhardt P., Eugster O., and Marti K. 1965. A redetermination of the isotopic composition of atmospheric neon. *Zeitschrift Naturforschung Teil A* 20: 623–624.

Eugster O. and Michel T. 1995. Common asteroid break-up events of eucrites, diogenites, and howardites and cosmic-ray production rates for noble gases in achondrites. *Geochimica et Cosmochimica Acta* 59:177–199.

Eugster O., Weigel A., and Polnau E. 1997. Ejection times of Martian meteorites. *Geochimica et Cosmochimica Acta* 61:2749–2757.

Eugster O., Busemann H., Lorenzetti S., and Terribilini D. 2002. Ejection ages from krypton-81-krypton-83 dating and pre-atmospheric sizes of Martian meteorites. *Meteoritics & Planetary Science* 37:1345–1360.

Franchi I. A., Wright I. P., Sexton A. S., and Pillinger C. T. 1999. The oxygen-isotopic composition of Earth and Mars. *Meteoritics & Planetary Science* 34:657–661.

Fritz J., Artemieva N., and Greshake A. 2005. Ejection of Martian meteorites. *Meteoritics & Planetary Science* 40:1393–1411.

Garrison D. H. and Bogard D. D. 1998. Isotopic composition of trapped and cosmogenic noble gases in several Martian meteorites. *Meteoritics & Planetary Science* 33:721–736.

Garrison D. H. and Bogard D. D. 2000. Cosmogenic and trapped noble gases in the Los Angeles Martian meteorite. *Meteoritics & Planetary Science* 35:A58.

Garrison D. H., Rao M. N. and Bogard D. D. 1995. Solar-proton-produced neon in shergottite meteorites and implications for their origin. *Meteoritics* 30:738–747.

Goodrich C. A. 2002. Olivine-phyric Martian basalts: A new type of shergottite. *Meteoritics & Planetary Science* 37: B31–B34.

Heber V. S., Wieler R., Baur H., Olinger C., Friedmann T. A., and Burnett D. S. 2009. Noble gas composition of the solar wind as collected by the Genesis mission. *Geochimica et Cosmochimica Acta* 73:7414–7432.

Honda M. and Imamura M. 1971. Half-life of ^{53}Mn. *Physical Review C* 4:1182–1188.

Ikeda Y., Kimura M., Takeda H., Shimoda G., Kita N. T., Morishita Y., Suzuki A., Jagoutz E., and Dreibus G. 2006. Petrology of a new basaltic shergottite: Dhofar 378. *Antarctic Meteorite Research* 19:20–44.

Irving A. 2011. Martian meteorites. http://www.imca.cc/mars/martian-meteorites. htm.

Jambon A., Barrat J. A., Sautter V., Gillet P., Göpel C., Javoy M., Loron J. L., and Lesourd M. 2002. The basaltic shergottites Northwest Africa 856: Petrology and chemistry. *Meteoritics & Planetary Science* 37:1147–1164.

Knie K., Faestermann T., Korschinek G., Rugel G., Rühm W., and Wallner C. 2000. High-sensitivity AMS for heavy nuclides at the Munich Tandem accelerator. *Nuclear Instruments and Methods in Physics Research B* 172:717–720.

Korschinek G., Bergmaier A., Faestermann T., Gerstmann U. C., Knie K., Rugel G., Wallner A., Dillmann I., Dollinger G., Lierse von Gostomski C., Kossert K., Maiti M., Poutivtsev M., and Remmert A. 2010. A new value for the half-life of ^{10}Be by heavy-ion elastic recoil detection and liquid scintillation counting. *Nuclear Instruments and Methods in Physics Research B* 268:187–191.

Lee J.-Y., Marti K., Severinghaus J. P., Kawamura K., Yoo H.-S., Lee J. B., and Kim J. S. 2006. A redetermination of the isotopic abundances of atmospheric Ar. *Geochimica et Cosmochimica Acta* 70:4507–4512.

Leya I. and Masarik J. 2009. Cosmogenic nuclides in stony meteorites revisited. *Meteoritics & Planetary Science* 44:1061–1086.

Lindsley D. H., Papike J. J., and Bence A. E. 1972. Pyroxferroite: Breakdown at low pressure and high temperature (abstract). 3rd Lunar Science Conference. p. 483.

Llorca J., Gich M., and Molins E. 2007. The Villalbeto de la Pena meteorite fall: III. Bulk chemistry, porosity, magnetic properties, Fe^{57} Mössbauer spectroscopy, and Raman spectroscopy. *Meteoritics & Planetary Science* 42:A177–A182.

Llorca J., Casanova I., Trigo-Rodríguez J. M., Madiedo J. M., Roszjar J., Bischoff A., Ott U., Franchi I., Greenwood R., and Laubenstein M. 2009. The Puerto Lápice eucrite. *Meteoritics & Planetary Science* 44:159–174.

Lodders K. 1998. A survey of shergottite, nakhlite and chassigny meteorites whole-rock compositions. *Meteoritics & Planetary Science* 33:A183–A190.

Mathew K. J. and Marti K. 2001. Early evolution of Martian volatiles: Nitrogen and noble gas components in ALH 84001 and Chassigny. *Journal of Geophysical Research* 106:1401–1422.

Mathew K. J., Marty B., Marti K., and Zimmermann L. 2003. Volatiles (nitrogen, noble gases) in recently discovered SNC meteorites, extinct radioactivities and evolution. *Earth and Planetary Science Letters* 214:27–42.

McLennan S. M. 2003. Large-ion lithophile element fractionation during the early differentiation of Mars and the composition of the Martian primitive mantle. *Meteoritics & Planetary Science* 38:895–904.

McSween H. Y., Jr. 1994. What we have learned about Mars from SNC meteorites—Invited review. *Meteoritics* 29:757–779.

McSween H. Y., Jr. 2002. The rocks of Mars, from far and near. *Meteoritics & Planetary Science* 37:7–25.

McSween H. Y., Jr. and Treiman A. H. 1998. Martian meteorites. In *Planetary materials*, edited by Papike J. J. Reviews in Mineralogy, vol. 36. Washington, D.C.: Mineralogical Society of America. pp. 6-1–6-53.

Merchel S., and Bremser W. 2004. First international ^{26}Al interlaboratory comparison—Part I. *Nuclear Instruments and Methods in Physics Research B* 223–224:393–400.

Merchel S. and Herpers U. 1999. An update on radiochemical separation techniques for the determination of long-lived radionuclides via accelerator mass spectrometry. *Radiochimica Acta* 84:215–219.

Merchel S., Bremser W., Akhmadaliev S., Arnold M., Aumaître G., Bourlès D. L., Braucher R., Caffee M., Christl M., Fifield L. K., Finkel R. C., Freeman S. P. H. T., Ruiz-Gómez A., Kubik P. W., Martschini M., Rood D. H., Tims S. G., Wallner A., Wilcken K. M., and Xu S. 2012. Quality assurance in accelerator mass spectrometry: Results from an international round-robin exercise for ^{10}Be. *Nuclear Instruments and Methods in Physics Research B* 289:68–73.

Mikouchi T. 2000. Pyroxene and plagioclase in the Los Angeles Martian meteorite: Comparison with the Queen Alexandra Ranche 94201 Martian meteorite and the Asuka 881757 lunar meteorite (abstract). *Meteoritics & Planetary Science* 35:A110.

Mikouchi T. 2001. Mineralogical similarities and differences between the Los Angeles basaltic shergottite and the Asuka-881757 lunar mare meteorite. *Antarctic Meteorite Research* 14:1–20.

Mohapatra R. K., Schwenzer S. P., and Ott U. 2002. Krypton and xenon in Martian meteorites from hot deserts—The low temperature component (abstract #1532). 33rd Lunar and Planetary Science Conference. CD-ROM.

Mohapatra R. K., Schwenzer S. P., Herrmann S., Murty S. V. S., Ott U., and Gilmour J. D. 2009. Noble gases and nitrogen in Martian meteorites Dar al Gani 476, Sayh al Uhaymir 005 and Lewis Cliff 88516: EFA and extra neon. *Geochimica et Cosmochimica Acta* 73:1505–1522.

Neal C. R., Taylor L. A., Ely J. C., Jain J. C., and Nazarov M. A. 2001. Detailed geochemistry of new shergottite, Dhofar 019 (abstract #1658). 32nd Lunar and Planetary Science Conference. CD-ROM.

Nishiizumi K., Caffee M. W., and Masarik J. 2000. Cosmogenic radionuclides in the Los Angeles Martian meteorite (abstract). *Meteoritics & Planetary Science* 35: A120.

Nishiizumi K., Imamura M., Caffee M. W., Southon J. R., Finkel R. C., and McAninch J. 2007. Absolute calibration of ^{10}Be AMS standards. *Nuclear Instruments and Methods in Physics Research B* 258:403–413.

Norris T. L., Gancarz A. J., Rokop D. J., and Thomas K. W. 1983. Half-life of ^{26}Al. Proceedings, 14th Lunar and Planetary Science Conference. *Journal of Geophysical Research Supplement 88:B331.*

Nyquist L. E., Reese Y. D., Wiesmann H., Shih C.-Y., and Schwandt C. 2000. Rubidium-strontium age of the Los Angeles shergottite. *Meteoritics & Planetary Science* 35: A121–A122.

Nyquist L. E., Bogard D. D., Shih C.-Y., Greshake A., Stöffler D., and Eugster O. 2001. Ages and geologic histories of Martian meteorites. *Space Science Reviews* 96:105–164.

Ott U. 1988. Noble gases in SNC meteorites: Shergotty, Nakhla, Chassigny. *Geochimica et Cosmochimica Acta* 52:1937–1948.

Ott U. and Löhr H. P. 1992. Noble gases in the new shergottite LEW 88516. *Meteoritics* 27:271.

Owen T., Biemann K., Rushneck D. R., Biller J. E., Howarth D. W., and Lafleur A. L. 1977. The composition of the atmosphere at the surface of Mars. *Journal of Geophysical Research* 82:4635–4640.

Pack A., Toulouse C., and Przybilla R. 2007. Determination of oxygen triple isotope ratios of silicates without cryogenic separation of NF_3—Technique with application to analyses of technical O_2 gas and meteorite classification. *Rapid Communications in Mass Spectrometry* 21:3721–3728.

Pepin R. O. 1991. On the origin and early evolution of terrestrial planet atmospheres and meteoritic volatiles. *Icarus* 92:2–79.

Poutivtsev M., Dillmann I., Faestermann T., Knie K., Korschinek G., Lachner J., Meier A., Rugel G., and Wallner A. 2010. Highly sensitive AMS measurements of ^{53}Mn. *Nuclear Instruments and Methods in Physics Research B* 268:756–758.

Reedy R. C. 1992. Solar-proton production of neon and argon. Proceedings, 23rd Lunar and Planetary Science Conference. pp. 1133–1134.

Rubin A. E., Warren P. H., Greenwood J. P., Verish R. S., Leshin L. A., Hervig R. L., Clayton R. N., and Mayeda T. K. 2000. Los Angeles: The most differentiated basaltic Martian meteorite. *Geology* 28:1011–1014.

Rugel G., Faestermann T., Knie K., Korschinek G., Poutivtsev M., Schumann D., Kivel N., Günther-Leopold I., Weinreich R., and Wohlmuther M. 2009. New measurement of the ^{60}Fe half-life. *Physical Review Letters* 103:072502.

Schaefer J. M., Faestermann T., Herzog G. F., Knie K., Korschinek G., Masarik J., Meier A., Poutitsev M., Rugel G., Schlüchter C., Serefiddin F., and Winckler G. 2006. Terrestrial ^{53}Mn—A new monitor of Earth surface processes. *Earth and Planetary Science Letters* 251:334–345.

Schwenzer S. P., Herrmann S., Mohapatra R. K., and Ott U. 2007. Noble gases in mineral separates from three shergottites: Shergotty, Zagami and EETA79001. *Meteoritics & Planetary Science* 42:387–412.

Schwenzer S. P., Fritz J., Stöffler D., Trieloff M., Amini M., Greshake A., Herrmann S., Herwig K., Jochum K. P., Mohapatra R. K., Stoll B., and Ott U. 2008. Helium loss from Martian meteorites mainly induced by shock metamorphism: Evidence from new data and a literature compilation. *Meteoritics & Planetary Science* 43:1841–1859.

Sharp Z. D. 1990. A laser-based microanalytical method for the *in situ* determination of oxygen isotope ratios of silicates and oxides. *Geochimica et Cosmochimica Acta* 54:1353–1357.

Shirai N. and Ebihara M. 2004. Chemical characteristics of a Martian meteorite, Yamato 980459. *Antarctic Meteorite Research* 17:55–67.

Smith J. V. and Hervig R. L. 1979. Shergotty meteorite: Mineralogy, petrography and minor elements. *Meteoritics* 14:121–142.

Smith S. P. and Huneke J. C. 1975. Cosmogenic neon produced from sodium in meteoritic minerals. *Earth and Planetary Science Letters* 27:191–199.

Stelzner T., Heide K., Bischoff A., Weber D., Scherer P., Schultz L., Happel M., Schrön W., Neupert U., Michel R., Clayton R. N., Mayeda T. K., Bonani G., Haidas I., Ivy-Ochs S., and Sutter M. 1999. An interdisciplinary study of weathering effects in ordinary chondrites from the Acfer region, Algeria. *Meteoritics & Planetary Science* 34:787–794.

Stöffler D., Keil K., and Scott E. R. D. 1991. Shock metamorphism of ordinary chondrites. *Geochimica et Cosmochimica Acta* 55:3845–3867.

Swindle T. D. 2002. Martian noble gases. In *Noble gases in geochemistry and cosmochemistry*, edited by Porcelli D., Ballentine C. J. and Wieler R. Reviews in Mineralogy and Geochemistry, vol. 47. Washington, D.C.: Mineralogical Society of America. pp. 171–190.

Swindle T. D., Caffee M. W., and Hohenberg C. M. 1986. Xenon and other noble gases in shergottites. *Geochimica et Cosmochimica Acta* 50:1001–1015.

Taylor L. A., Nazarov M. A., Shearer C. K., McSween H. Y. Jr., Cahill J., Neal C. R., Ivanova M. A., Barsukova L. D., Lentz R. C., Clayton R. N., and Maayeda T. K. 2002. Martian meteorite Dhofar 019: A new shergottite. *Meteoritics & Planetary Science* 37:1107–1128.

Terribilini D., Busemann H., and Eugster O. 2000. Krypton-81-krypton CRE ages of Martian meteorites including the new shergottite Los Angeles. *Meteoritics & Planetary Science* 35:A155–A156.

Vogel N., Heber V. S., Baur H., Burnett D. S., and Wieler R. 2011. Argon, krypton, and xenon in the bulk solar wind as collected by the Genesis mission. *Geochimica et Cosmochimica Acta* 75:3057–3071.

Walton E. L. and Herd C. D. K. 2007. Localized shock melting in lherzolitic shergottite Northwest Africa 1950: Comparison with Allan Hills 77005. *Meteoritics & Planetary Science* 42:63–80.

Walton E. L., Jugo P. J., Herd C. D. K., and Wilke M. 2010. Martian regolith in Elephant Moraine 79001 shock melts? Evidence from major element composition and sulfur speciation. *Geochimica et Cosmochimica Acta* 74:4829–4843.

Warren P. H., Greenwood J. P., Richardson J. W., Rubin A. E., and Verish R. S. 2000. Geochemistry of Los Angeles, a ferroan, La- and Th-rich basalt from Mars (abstract #2001). 31st Lunar and Planetary Science Conference. CD-ROM.

Warren P. H., Greenwood J. P., and Rubin A. E. 2004. Los Angeles: A tale of two stones. *Meteoritics & Planetary Science* 39:137–156.

Wieler R. 2002. *Cosmic-ray-produced noble gases in meteorites, Noble gases in geochemistry and cosmochemistry*. Washington, D.C.: Geochemical Society. pp. 125–170.

Wiens R. C. 1988. Noble gases released by vacuum crushing of EETA79001 glass. *Earth and Planetary Science Letters* 91:55–65.

Wiens R. C., Becker R. H., and Pepin R. O. 1986. The case for a Martian origin of the shergottites II: Trapped and indigenous gas components in EETA79001 glass. *Earth and Planetary Science Letters* 77:149–158.

Xirouchakis D., Draper D. S., Schwandt C. S., and Lanzirotti A. 2002. Crystallization conditions of Los Angeles, a basaltic Martian meteorite. *Geochimica et Cosmochimica Acta* 66:1867–1880.

Young E. D., Galy A., and Nagahara H. 2002. Kinetic and equilibrium mass-dependent isotope fractionation laws in nature and their geochemical and cosmochemical significance. *Geochimica et Cosmochimica Acta* 66:1095–1104.

Zipfel J., Scherer P., Spettel B., Dreibus G., and Schultz L. 2000. Petrology and chemistry of new shergottite Dar al Gani 476. *Meteoritics & Planetary Science* 35:95–106.